

Advances in modeling the flow of Herschel-Bulkley fluids in pipes

A review

Yusufi, B. K.; Kapelan, Z.; Mehta, D.

DOI

[10.1063/5.0252248](https://doi.org/10.1063/5.0252248)

Publication date

2025

Document Version

Final published version

Published in

Physics of Fluids

Citation (APA)

Yusufi, B. K., Kapelan, Z., & Mehta, D. (2025). Advances in modeling the flow of Herschel-Bulkley fluids in pipes: A review. *Physics of Fluids*, 37(2), Article 021302. <https://doi.org/10.1063/5.0252248>

Important note

To cite this publication, please use the final published version (if applicable). Please check the document version above.

Copyright




Other than for strictly personal use, it is not permitted to download, forward or distribute the text or part of it, without the consent of the author(s) and/or copyright holder(s), unless the work is under an open content license such as Creative Commons.

Takedown policy

Please contact us and provide details if you believe this document breaches copyrights. We will remove access to the work immediately and investigate your claim.

REVIEW ARTICLE | FEBRUARY 11 2025

Advances in modeling the flow of Herschel–Bulkley fluids in pipes: A review

B. K. Yusufi ; Z. Kapelan ; D. Mehta 



Physics of Fluids 37, 021302 (2025)

<https://doi.org/10.1063/5.0252248>



Articles You May Be Interested In

Unsteady solute dispersion in Herschel-Bulkley fluid in a tube with wall absorption

Physics of Fluids (November 2016)

Rheology-based wall function approach for wall-bounded turbulent flows of Herschel–Bulkley fluids

Physics of Fluids (February 2024)

On the determination of yield surfaces in Herschel–Bulkley fluids

J. Rheol. (May 1999)



Physics of Fluids

Special Topics Open
for Submissions

[Learn More](#)

Advances in modeling the flow of Herschel–Bulkley fluids in pipes: A review

Cite as: Phys. Fluids **37**, 021302 (2025); doi: [10.1063/5.0252248](https://doi.org/10.1063/5.0252248)

Submitted: 8 December 2024 · Accepted: 9 January 2025 ·

Published Online: 11 February 2025



View Online



Export Citation



CrossMark

B. K. Yusufi,^{a)}  Z. Kapelan,  and D. Mehta 

AFFILIATIONS

Section Sanitary Engineering, Department of Water Management, Faculty of Civil Engineering, Delft University of Technology, Stevinweg 1, Delft, 2628 CN, The Netherlands

^{a)} Author to whom correspondence should be addressed: b.k.yusufi@tudelft.nl

ABSTRACT

This review explores recent advancements in modeling the flow behavior of Herschel–Bulkley (HB) fluids in pipes, discussing theoretical, semi-empirical, computational, and experimental methods. While the laminar flow of non-Newtonian HB fluids can be effectively modeled using first-principle physics, significant challenges remain in turbulent and transitional flow regimes. Existing turbulence models, though widely used, may not always fully align with experimental data, often requiring further validation or complex mathematical tuning, leading to higher computational costs. Further, the transition to turbulence in HB fluids is influenced by shear-thinning and yield stress, yet current models often fail to account for this delayed transition. Consequently, stability and Reynolds number-based transition models can exhibit inconsistencies, limiting their broader applicability. Progress is further hindered by limited experimental studies, constrained by resolution, attenuation, cost, and material combinations. Inaccuracies in rheological modeling—due to inappropriate shear rate ranges, curve-fitting techniques, or simplifying assumptions such as homogeneity and non-elasticity—further complicate flow predictions. Through this review, we delve deeper into the state-of-the-art modeling of HB fluids, highlighting progress and these challenges. Addressing these limitations requires advanced experimental and numerical studies, particularly for near-wall measurements, to better capture flow complexities and improve model predictions. This could also facilitate the development of data-driven approaches and operational envelopes that define their validity thresholds. Future research should also prioritize the independent effects of yield stress and shear-thinning properties while considering material attributes and settling phenomena in non-Newtonian suspensions. Ultimately, these advancements will enable more accurate flow predictions and practical solutions for industrial applications.

© 2025 Author(s). All article content, except where otherwise noted, is licensed under a Creative Commons Attribution (CC BY) license (<https://creativecommons.org/licenses/by/4.0/>). <https://doi.org/10.1063/5.0252248>

I. INTRODUCTION

Fluid transportation through pipelines is a cornerstone of modern infrastructure, playing a pivotal role both in public services such as water distribution, sanitation, and water treatment, as well as in industries including agriculture, chemicals, mining, dredging, oil, and gas. Supporting both long-distance transport and processing, this method is often cost-effective, time-efficient, and particularly reliable in remote areas, especially for transporting hazardous or radioactive materials (Kujawa-Roeleveld and Zeeman, 2006; Todt *et al.*, 2021). Therefore, ensuring that pipeline transport remains energy-efficient and durable is important, highlighting the need for a comprehensive understanding of the underlying fluid dynamics.

Fluids can be broadly categorized as Newtonian or non-Newtonian based on their response to shear (Chhabra, 2010). Newtonian fluids exhibit a linear relationship between shear stress and shear rate, following Newton's law of viscosity. In contrast, non-

Newtonian fluids show a non-linear relationship and may require minimum shear stress (known as yield stress) to flow. Their viscosity depends on the local shear rate and can either decrease (thixotropy) or increase (rheopecty) under constant shear. Other factors, such as kinematic history, temperature, pressure, and elasticity, also influence their viscosity (Larson and Wei, 2019; Carreau *et al.*, 2021b).

For simplicity, non-Newtonian fluids are categorized into purely viscous, where viscosity depends on shear rate only; time-dependent, where viscosity changes over time; and viscoelastic fluids, which exhibit elastic recovery or solid-like behavior after deformation (Bird *et al.*, 1987). Figure 1 illustrates the classification of single-phase fluids based on their response to shear stress.

This article focuses on purely viscous, time-independent, non-Newtonian fluids with an emphasis on Herschel–Bulkley (HB) fluids. Therefore, in this context, “non-Newtonian” refers exclusively to time-independent fluids. Unless otherwise specified, discussions pertain to Herschel–Bulkley, Bingham-plastic (BP), or power-law (PL) fluids. For

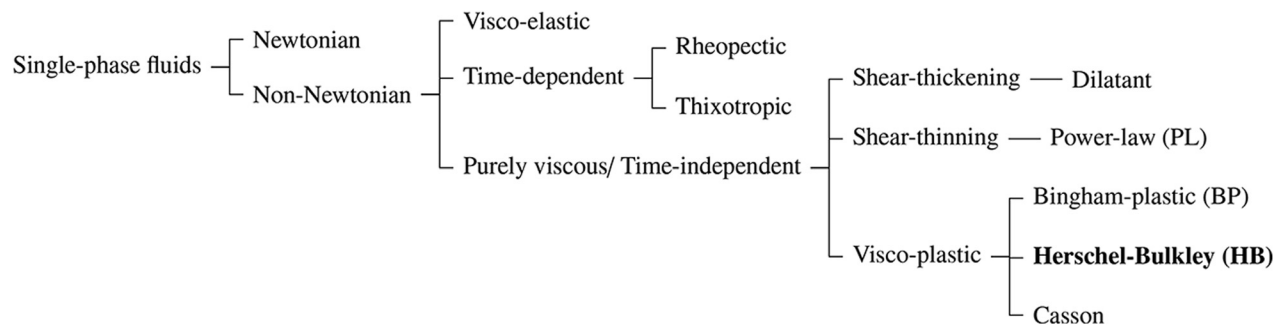


FIG. 1. Classification of fluids based on their response to shear.

more on time-dependent fluids, see Mewis (1979), Barnes (1997), Govier *et al.* (1973), and Livescu (2012), and for viscoelastic fluids, refer to reviews such as Bird *et al.* (1987), Morrison (2001), and Carreau *et al.* (2021a).

A. Pipe flow and Newtonian fluids

Efficient pipeline transport of fluids relies on quantifying parameters such as pressure loss due to wall friction, which determines the pumping capacity required for optimized flow conditions. Other key parameters include the velocity distribution across the cross section, turbulence intensity (to assess mixing and prevent settling), and thermal effects, which are important for chemical reactions and heat transfer to the pipes (Szilas *et al.*, 1981). These factors can be evaluated through full-scale pipe experiments or using mathematical models that combine theoretical and empirical approaches. Advances in computational technology have made it possible to perform numerical simulations based on the discrete form of the governing differential equations of fluid mechanics (Messa *et al.*, 2021). While experiments are considered the most reliable data source, their applicability is often limited by cost, time, resolution, rigidity, and instrument reliability (Bayareh, 2023). Consequently, academics and engineers increasingly seek alternative methods, such as theoretical, semi-empirical, and computational models, for determining pressure loss and estimating turbulence.

Over the years, Newtonian fluids, such as air and water, have received significant scientific attention, resulting in the development of models that accurately describe both laminar and turbulent flows. For instance, wall shear stress, a measure of viscous effects in laminar flow, can be calculated using the Hagen-Poiseuille equation, which relates pressure loss to velocity, pipe diameter, and molecular viscosity. Alternatively, for turbulent flows, semi-empirical equations developed by Blasius (1913), Nikuradse (1933), von Kármán (1931), Moody (1944), and Colebrook (1939) and computational models such as Launder and Spalding (1974) are used to estimate wall shear stress and pressure loss. Numerous experiments and applications have demonstrated the robustness of these models. In fact, Heywood and Cheng (1984) showed that variations between these turbulent Newtonian models remain within $\pm 4\%$, which simplifies model selection [details could be found in Rennels and Hudson (2012)].

B. Non-Newtonian fluids

The above anecdote is different for non-Newtonian fluids. As compared to their Newtonian counterparts, non-Newtonian fluids

have received limited scientific attention, resulting in a significant knowledge gap in the field of non-Newtonian fluid mechanics and its modeling (Lovato *et al.*, 2022b). Under laminar flow, the behavior of non-Newtonian fluids can be effectively modeled (with reasonable accuracy and reliability) using first-principle physics—applying fundamental laws without relying on assumptions or curve-fitting—in conjunction with appropriate rheological models (discussed in detail later).

However, modeling turbulent flows, which are frequently encountered in industrial settings, where non-Newtonian fluids are transported through large-diameter pipes at high flow rates (to prevent particle settling and clogging), presents a greater challenge. Such flows require the simultaneous consideration of both turbulence dynamics and the fluid's complex rheological behavior (Chilton and Stainsby, 1998). As discussed later, this modeling demands mathematical rigor, often simplified through assumptions and informed by experimental data, which remains limited. Hence, most methods are either limited to the parametric envelope defined by the experimental data used for tuning and validation or are incompatible with flows that demonstrate high levels of turbulence (as discussed later, most experimental evidence has been collected at low levels of turbulence). Through this review, we will explore the existing theoretical and computational models for the turbulent flow of HB fluids and discuss the above-mentioned limitations and potential areas for further improvement.

In Newtonian fluid mechanics, we observe that as flow velocity increases in the laminar regime, inertial forces gradually dominate viscous forces, leading to instabilities that can ultimately trigger turbulence (Eckert, 2021). The regime between laminar and turbulent flows, in which these instabilities develop and reinforce each other, is known as the transition regime. For non-Newtonian fluids, the complexity is further amplified due to shear thinning behavior, which prompts the delayed transition and asymmetries (Güzel *et al.*, 2009). Though recent advancements, such as the development of universal turbulence models capable of addressing laminar, transitional, and turbulent flows [e.g., Deng (2024)], have emerged, traditional engineering systems are still typically designed to operate in either fully laminar or fully turbulent regimes. This approach avoids the transitional range and helps mitigate issues such as particle settling, clogging, water hammer, cavitation, and accelerated pipe wear (Dash *et al.*, 2022; Visintainer *et al.*, 2023).

However, this approach necessitates the accurate determination of the transition zone, particularly the onset of transition from laminar behavior and the critical point at which the flow becomes fully

turbulent. While the Reynolds number serves as a reliable indicator for estimating this transition zone in Newtonian fluids (Madlener *et al.*, 2009), this approach is not directly applicable to non-Newtonian fluids due to their shear-dependent viscosity and/or yield stress (Singh *et al.*, 2018). In addition, experimental investigations face further constraints in terms of maximum measurable depth or flow velocities and limited material combinations due to the opaque nature of these fluids, attenuation, and high particle concentration (Poelma, 2020). This review will further explore how current models and experimental developments address these challenges and highlight gaps that still need to be filled.

Despite advancements in numerical simulations, data processing, and experimental techniques, a comprehensive review of the turbulent flow of HB fluids remains elusive. Foundational works by Skelland (1967), Govier *et al.* (1973), and Bird *et al.* (1987) offer fundamental perspectives on numerical methods, while Chhabra and Richardson (2008a) focus on analytical and semi-empirical approaches for PL and BP fluids primarily under laminar and transitional flows. Similarly, review articles by Heywood and Cheng (1984) and Assefa and Kaushal (2015) primarily address theoretical and semi-empirical methods. Recent reviews, such as those by Wang *et al.* (2023); Messa *et al.* (2021) and Alves *et al.* (2021); Livescu (2012), fall outside the present scope, focusing instead on multiphase slurries or viscoelastic fluids. Therefore, a comprehensive review that encompasses all available techniques for HB fluids, including those with potential for further advancement, is still lacking in scientific literature.

This article aims to address this gap by consolidating the existing literature on theoretical, semi-empirical, and computational approaches for modeling HB fluids in smooth pipes across all flow regimes—laminar, transitional, and turbulent. Particular focus is given to turbulent flows that are still ambiguous to researchers due to limited experimental data and significant uncertainties. The review also examines recent experimental developments and underscores the need for a similarity parameter, such as a Reynolds number equivalent, for non-Newtonian fluids. While the review acknowledges the challenges in rheological characterization, a detailed discussion is beyond the scope of this review. Readers seeking comprehensive insights into rheometry and rheological parameter estimation are encouraged to refer to Chhabra and Richardson (2008b) and Busch *et al.* (2019). Overall, this review identifies current gaps and uncertainties in the field, potentially laying the groundwork for future research.

The paper is structured as follows. Section I provides background and introduces the challenges in this field, while Sec. II describes HB fluids and various non-Newtonian Reynolds number models. Section III covers turbulent flow in detail, covering both semi-empirical and computational methods, followed by Sec. IV, which focuses on laminar-turbulent transition and a handful of models that are in use for estimating its onset. Section V briefly summarizes recent experimental developments. Finally, Sec. VI concludes the paper by highlighting knowledge gaps, and Sec. VII suggests possible avenues for further research.

II. HERSCHEL-BULKLEY FLUIDS AND FLOW BEHAVIOR

A. Herschel-Bulkley fluids

Herschel-Bulkley (HB) fluids exhibit yield pseudo-plastic behavior, characterized by distinct yield and post-yield behavior. Below the yield stress, HB fluids behave like solids. Once the local shear exceeds the yield stress, the post-yield behavior is non-linear, displaying shear-

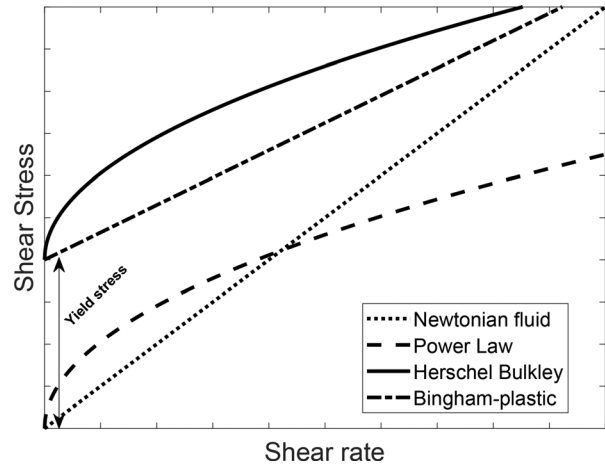


FIG. 2. Types of time-independent fluid behavior.

thinning properties, where the viscosity decreases with increasing shear rate (Chaudhuri *et al.*, 2005). Figure 2 shows a typical rheogram (shear stress vs shear rate) of an HB fluid. Mathematically, as proposed by Herschel and Bulkley (1926)

$$\tau = \tau_y + m\dot{\gamma}^n. \tag{1}$$

m is the consistency index and n is the behavior index. Equation (1) is applicable when the magnitude of the imposed shear stress ($|\tau|$ or τ) is greater than or equal to the yield stress, i.e., $|\tau| \geq \tau_y$. When $|\tau| < \tau_y$, the shear rate ($\dot{\gamma}$) is 0.

What is convenient about this equation is that it can be treated as a generalized equation for other established viscous time-independent non-Newtonian fluids. For instance, when $n = 1$, it represents a BP fluid; when $\tau_y = 0$, it reduces to a PL fluid; and when both $\tau_y = 0$ and $n = 1$, it simplifies to a Newtonian fluid, with the consistency index m representing the molecular viscosity μ (Gavrilov *et al.*, 2017; Lovato *et al.*, 2022a). This is also why the modeling approaches covered in the article concern HB fluids. Based on mathematical consistency, as shown above, all HB models can ultimately be adapted to BP, PL, and even Newtonian models.

In three dimensions and full tensor notation [as in Oldroyd (1947)], Eq. (1) reads

$$\tau = \left(\frac{\tau_y}{|\dot{\gamma}|} + m|\dot{\gamma}|^{n-1} \right) \dot{\gamma}, \tag{2}$$

where $|\dot{\gamma}|$ is the magnitude (the second invariant) of $\dot{\gamma}$ and equals

$$|\dot{\gamma}| = \sqrt{\frac{1}{2} \{\dot{\gamma} : \dot{\gamma}\}}, \tag{3}$$

$$\dot{\gamma} : \dot{\gamma} = \text{tr}(\dot{\gamma}^T \dot{\gamma}). \tag{4}$$

The term $\dot{\gamma} : \dot{\gamma}$ refers to the Frobenius product, which is essentially the sum of the element-wise products of two matrices (in this case, $\dot{\gamma}$ with itself). In simpler terms, it measures the “similarity” between the matrix and itself. Meanwhile, tr is the trace of a matrix, which is the sum of the diagonal elements, and T denotes the transpose of the matrix.

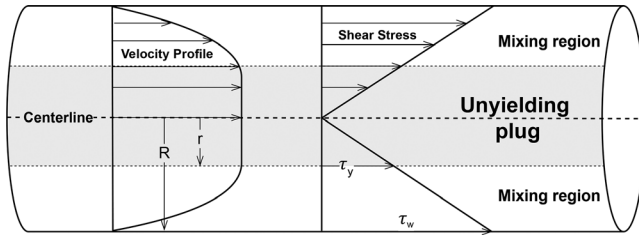


FIG. 3. Velocity profile for an HB fluid inside a pipe during laminar flow.

Now, at any radial distance r from the pipe’s axis, the shear stress τ_r can be modeled as a function of the shear rate $\dot{\gamma} = -du/dr$ according to

$$\tau_r = \begin{cases} \tau_y + m \left(\frac{-du}{dr} \right)^n & \text{if } |\tau| \geq \tau_y, \\ \tau_y & \text{if } |\tau| < \tau_y. \end{cases} \quad (5)$$

Equation (5) can further be integrated across the pipe’s diameter (refer to Fig. 3) to obtain the average velocity (U)

$$U = \frac{D}{2} \left(\frac{\tau_y}{m} \right)^{\frac{1}{n}} \left[\frac{n(1-\phi)}{\phi^n} \right] \times \left[\frac{(1-\phi)^2}{1+3n} + \frac{2\phi(1-\phi)}{1+2n} + \frac{\phi^2}{1+n} \right]. \quad (6)$$

For a given bulk velocity U (or volumetric flow rate), the above equation can be solved implicitly for the wall shear stress under laminar flow conditions. Please note that the approach outlined here provides only a concise overview of the velocity profile and wall shear stress for HB fluids under laminar flow. For a comprehensive derivation and more detailed discussion, readers are referred to the works of Skelland (1967), Govier *et al.* (1973), Escudier and Presti (1996), and Chhabra and Richardson (2008a).

B. Non-Newtonian Reynolds number

Non-Newtonian fluids, characterized by their shear rate-dependent viscosity, present an ambiguity in the choice of viscosity scale when using the conventional definition of the Reynolds number (Singh *et al.*, 2018). However, several attempts have been made to establish a similar relationship for non-Newtonian fluids. For instance, Rabinowitsch (1929) and Mooney (1931) demonstrated that for any fluid in laminar flow through a pipe, a unique relationship exists between the wall shear stress (τ_w) and the pseudo shear rate ($8U/D$). Building on this, Metzner and Reed (1955) proposed, generalized Metzner and Reed Reynolds number (Re_{MR})

$$Re_{MR} = \frac{8\rho U^2}{m \left(\frac{8U}{D} \right)^{n'}}. \quad (7)$$

Here, ρ denotes fluid density, U represents cross section averaged velocity, and D is inner pipe diameter. n' and m' are the apparent behavior and consistency indices, respectively, and can be evaluated as functions of the true n and m (obtained through rheological

experiments and model fitting). Graphically, n' and $\log(m')$ are the slope and intercept in a $\log(\tau_w) - \log(8U/D)$ plot, respectively.

Re_{MR} , though proposed for PL fluids, could also be extended to HB fluids while indirectly incorporating the yield stress through m' and n' . A clear advantage of using Re_{MR} is that the Moody chart (developed and well-adapted for Newtonian fluids) could be used for non-Newtonian fluids. However, this definition has certain limitations. For instance, Metzner and Reed assumed that m' and n' remain constant over a wide range of shear stresses. While this assumption holds for PL fluids, where m' and n' are independent of τ_w , Lazarus and Slatter (1988) demonstrated that it does not apply to HB fluids, requiring m' and n' to be evaluated at each specific τ_w , complicating the process. Additionally, their expression was derived from laminar flow analysis and is thus inadequate for turbulent flow conditions (Güzel *et al.*, 2009; Singh *et al.*, 2018).

Chilton and Stainsby (1998) and later Rudman *et al.* (2004) sought to address these limitations by using apparent wall viscosity (η_w), which accounts for variations in wall shear stress influencing near-wall viscosity, a critical factor in the turbulent characteristics of wall-bounded flows such as pipes. The Reynolds number (Re_w) as proposed by Rudman *et al.* (2004) is

$$Re_w = \frac{\rho U D}{\eta_w}. \quad (8)$$

η_w is determined by rearranging Eq. (1) as follows:

$$\eta_w = m^{1/n} \frac{\tau_w}{(\tau_w - \tau_y)^{1/n}}. \quad (9)$$

Similarly, various other definitions for non-Newtonian Reynolds numbers have been proposed in the literature, such as Tomita (1959), Clapp (1961), Slatter (1996), and Madlener *et al.* (2009). Readers are encouraged to refer to Haldenwang *et al.* (2012) for a detailed discussion and comparison of these Reynolds number models. However, there remains a lack of consensus or comprehensive studies comparing these models to ascertain their applicability under specific conditions.

Further, these Reynolds number models often demonstrate inconsistencies. For instance, Yusufi *et al.* (2024) noted that laminar flow persisted even at Re_w exceeding 8000. Similarly, a recent experimental study by Charles *et al.* (2024) highlighted that the shear-thinning behavior and yield stress of HB fluids could delay the transition to turbulence (in their experiments, it was at $Re_w = 6260$). Other experimental studies such as Güzel *et al.* (2009) have shown that the turbulent transition in non-Newtonian fluids occurs across a broad range of Reynolds numbers, not at a single defined value (discussed in detail in Sec. IV). However, the predicted upper-bound and lower-bound values of the Reynolds number to distinguish between the different flow behaviors are highly inconsistent.

Consequently, the original purpose of the Reynolds number, which was to provide an indication of the flow regime—becomes less reliable with these fluids. As one might expect, the difficulty in theoretically modeling the flow regime arises from the shear-dependent viscosity and the dependency on pipe diameter inherent to non-Newtonian fluids. Additionally, semi-empirical correlations are often highly localized, limiting their broader applicability. As a result, the numerical values of these modified Reynolds numbers may lack universal meaning, always requiring experimental validation (Draad *et al.*, 1998). Also, these turbulent Reynolds numbers correlations are based

on wall viscosity, which depends on wall shear stress—an initially unknown parameter, further complicating their practical application.

III. TURBULENT FLOWS OF HB FLUIDS

Modeling non-Newtonian turbulent flows is more intricate than Newtonian flows, as fluctuations in the velocity field cause changes in the local shear rates, which in turn affect the local viscosity. This viscosity, which depends on the shear rate, can dampen the turbulent structures, altering the shear rate again and further changing the viscosity. Taking into account for this effect involves a rigorous mathematical exercise, combining two models: one for characterizing the turbulence effects and the other for defining the rheology of the fluid (Chilton and Stainsby, 1998). Both models are coupled in the sense that they affect each other simultaneously. Various methods have been proposed in the literature to model this interaction, which is discussed in this section.

A. Semi-empirical models

Researchers have defined turbulence in non-Newtonian fluids using analogies with Newtonian fluids, rooted in the fact that the velocity profile in the turbulent core region is more governed by turbulent momentum transfer rather than viscosity (Wilson and Thomas, 1985). This strong similarity in the turbulent velocity profiles between Newtonian and non-Newtonian fluids has been established in the past both theoretically (Skelland, 1967; Govier et al., 1973; and Slatter, 1996) and experimentally (Park et al., 1989a; Escudier and Presti, 1996; Peixinho et al., 2005; and Mitishita et al., 2021).

To establish a relationship between turbulent flows in Newtonian and non-Newtonian fluids, the analysis can be divided into two main steps. The first step involves developing a turbulence model. Near the wall, the turbulent boundary layer of a Newtonian fluid can be divided into three distinct regions (refer to Fig. 4). These include the viscous sub-layer, which is closest to the surface and where viscosity dominates turbulence; the buffer layer, which serves as a transition zone where both effects are significant; and the fully turbulent log-law layer, where turbulence effects dominate; and the velocity profile follows a logarithmic scale (Dewan, 2011).

The viscous sub-layer has steady laminar conditions, which means a linear, analytically derived velocity profile. This enables one to

assume a constant viscosity equal to the wall viscosity, which can be expressed in a parametric (non-dimensional) form as

$$u^+ = y^+ \tag{10}$$

Here, $u^+ = u/u_\tau$, $y^+ = yu_\tau/\nu$ are the non-dimensional velocity and normal distance from the wall, respectively, ν is the kinematic viscosity defines for Newtonian fluids, and u_τ is the shear velocity defined as

$$u_\tau = \sqrt{\frac{\tau_w}{\rho}} \tag{11}$$

In the turbulent or the log-law layer away from the wall, the velocity (parallel to the wall) follows a logarithmic profile (here, κ is the von Karman constant)

$$u^+ = \frac{1}{\kappa} \ln y^+ + B \tag{12}$$

An analogous equation for non-Newtonian fluids has been established in the literature (Govier et al., 1973; Bogue and Metzner, 1963) and experimentally demonstrated in (Xu et al., 1993; Park et al., 1989a). This shared characteristic supports the assumption that the velocity distribution away from the walls of a pipe carrying non-Newtonian fluids in turbulent flow follows a logarithmic profile (for most of the pipe’s cross section) akin to Newtonian fluids in turbulent flow.

The next and more intricate step involves incorporating rheological properties into the existing turbulence model. This integration is accomplished through various approaches, including empirical data, semi-empirical formulas, and theoretical models. For instance, Tomita (1959) used the well-known mixing length theory put forth by Prandtl (1926) to describe the turbulent flow of non-Newtonian fluids. Tomita treated the turbulent flows of PL and BP fluids as imaginary laminar flows with an average velocity equal to the turbulent flow velocity and derived model constants using experimental data. This approach was later extended to HB fluids by Mehta et al. (2021). However, the overall methodology has not been positively validated using independent experimental data, leading to disparate predictions as highlighted in various literature (Heywood and Cheng, 1984; Chhabra and Richardson, 2008a; and Mehta et al., 2021).

Dodge and Metzner (1959) defined a semi-empirical approach for PL fluids, using dimensional analysis and correlations with Newtonian turbulent flows [as done in Nikuradse (1933)] to derive a logarithmic velocity profile and friction factor expression. This approach could be extended to any non-Newtonian fluid by deriving apparent behavior (n') and consistency (m') indices from a shear stress-shear rate curve (Rabinowitsch-Mooney principle, see Sec. II B). This process is straightforward for PL fluids with constant n' and m' values. However, it becomes more intricate for HB fluids due to yield stress; the values of n' and m' depend on the unknown τ_w . The procedure involves an initial assumption of τ_w followed by an iterative approach to solve the above correlation. Nevertheless, there are no established guidelines for accurately predicting or assuming the correct value of τ_w beforehand, limiting the approach to PL fluids.

Torrance (1963) derived the turbulent velocity profiles in smooth pipes for HB fluids, using the generalized Reynolds number proposed by Clapp (1961) for PL fluids. In their approach, they used the mixing length model to define turbulence and a modified value of the Von-

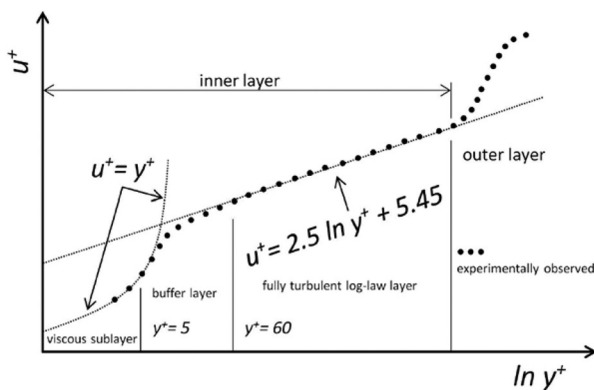


FIG. 4. Law of the wall for Newtonian Fluids. Adapted from ANSYS (2024).

Karman constant to account for the HB viscosity. Further, Hanks [Hanks \(1978\)](#) proposed a theoretical framework to model turbulent HB flow, aiming to create friction factor–Reynolds number curves similar to the Moody chart for Newtonian fluids. Hanks' method also incorporates a modified form of the Prandtl mixing length model; however, that includes an empirical wall effect parameter (B) instead, influenced by the Hedstrom number (He), which is the ratio of yield stress to viscous forces in HB fluids.

Later, Wilson & Thomas proposed a theoretical approach for PL and BP fluids ([Wilson and Thomas, 1985](#)) and subsequently for HB fluids ([Thomas and Wilson, 1987](#)). They proposed that turbulence in such fluids is driven by the formation of micro eddies, categorized into two: dissipative micro eddies found in the laminar (or viscous) sub-layer and inertial micro eddies in the turbulent core. As fluids become more non-Newtonian, the size of dissipative micro-eddies increases, leading to a corresponding increase in the thickness of the laminar sub-layer. This change in structure increases the velocity within the fluid, promoting drag reduction—a phenomenon previously observed and reported by [Dodge and Metzner \(1959\)](#) concerning turbulent systems. They established a relationship between the thickness of the viscous sub-layer and the area ratio (a), defined as the ratio of the area under the non-Newtonian Rheogram (Shear stress vs Shear Rate plot, see [Fig. 2](#)) to that for a Newtonian fluid under the same shear rate range. These areas can be directly obtained from the Rheogram without the need to fit any rheological models, thus simplifying the analysis.

Subsequently, [Slatter \(1996\)](#) considers non-Newtonian fluids composed of solid particles (typically sand) that cause a reduced velocity gradient near a wall. The solid particles are assumed to induce a roughness effect that can mathematically be modeled as increased pipe roughness. A logarithmic Newtonian turbulent velocity profile is adapted to describe non-Newtonian fluids in turbulent flow. The reduced velocity gradient (due to the particles) is modeled using a roughness Reynolds number (Re_r), which is a function of the fluid's rheological parameters n , m , and τ_y . The representative size of particles d_x is chosen based on sensitivity analysis and minimum wall shear stress prediction error. The aforementioned models and their respective formulations are summarized in [Table 1](#).

Despite these contributions, the above-discussed correlations have certain limitations. For instance, models proposed by [Torrance \(1963\)](#), [Wilson and Thomas \(1985\)](#), and [Thomas and Wilson \(1987\)](#) were found to be accurate at the early stage of turbulence but were sensitive to rheological parameters as reported in [Slatter \(1996\)](#). Slatter made a few assumptions, such as the impact of particles near the wall leading to a reduction in velocity gradient akin to pipe roughness and the utilization of the representative particle size (d_{85}), which lacks a solid theoretical foundation. Also, the assumption that the plug flow abruptly disappears at the critical Reynolds number during the transition from laminar to turbulent flow contradicts Bowen's findings ([Bowen, 1961](#)) and experimental observations by [Peixinho et al. \(2005\)](#).

Hanks's approach, despite being used in various studies, including recent ones ([Nizamidin, 2016](#); [Rojas and Janssen, 2013](#)), lacks experimental validation and theoretical support, particularly concerning the definition of the wall effect parameter B . This issue has been highlighted in studies such as [Bharathan et al. \(2019\)](#), which observed that the Hanks model underpredicts the friction factor, possibly due to the empirical nature of the expression. In addition, the method is also

known to be time and resource-intensive to execute and involves a series of steps before the desired friction factor or wall shear stress is determined ([Rao, 2014](#)). The inherent complexity of non-Newtonian behavior, combined with the limited understanding of turbulence in such fluids, significantly restricts the applicability of these semi-empirical models. Consequently, these models could often produce predictions that deviate by more than $\pm 50\%$ from experimental observations ([Heywood and Cheng, 1984](#)).

For instance, [Assefa and Kaushal \(2015\)](#) conducted a comparative study of friction factor correlations for high-concentration slurry flow in smooth pipes, focusing on BP fluids. They reported that Slatter's model performed poorly, especially in turbulent flow regimes, while the Wilson and Thomas model was highly accurate up to Reynolds numbers of 40 000, beyond which its accuracy declined. [Mehta et al. \(2021\)](#) conducted a comprehensive comparison of wall shear stress predictions of HB fluids from semi-empirical models, including Dodge & Metzner, Tomita, Torrance, Wilson & Thomas, and Slatter, using eight experimental datasets from [Krishnan Thota Radhakrishnan et al. \(2018\)](#) and [Slatter \(1996\)](#). The probability of predicting the wall shear stress within a 95% confidence limit was calculated to evaluate the performance of these models. They concluded that while most existing models deliver estimates of comparable accuracy, the probability of these estimates being reliable while accounting for experimental errors in quantifying the actual frictional losses is rather low, with the maximum being 0.27 [see [Fig. 5\(a\)](#)].

Recently, [Yusufi et al. \(2024\)](#) compared the velocity profiles and concluded that none of these models are universally applicable across the entire range of turbulent flow for HB fluids. Both Torrance and Wilson and Thomas's models were highly sensitive to changes in viscosity near the wall and were only accurate in the early stages of turbulence, diverging significantly at high Reynolds numbers (consistent with Mehta's and Slatter's findings). Slatter's model, however, was found to be the most accurate in regions where the laminar sub-layer became thin, and micro-eddies and particles significantly influenced the velocity distribution [see [Fig. 5\(b\)](#)]. Dodge and Metzner under-predicted wall shear stress across all Reynolds numbers. Contrarily, studies such as those by [El-Emam et al. \(2003\)](#), [Gul et al. \(2019\)](#), and [Sorgun et al. \(2022\)](#) found that the Dodge and Metzner correlation tended to overestimate friction factors.

These discrepancies largely stem from underlying assumptions, oversimplifications, or limited training datasets, as highlighted in [Yousuf et al. \(2024\)](#), making these semi-empirical correlations far from universal. Other correlations, such as those involving rough pipes, discussed by [Szilas et al. \(1981\)](#), are beyond the scope of this paper and will not be discussed in detail. For a more comprehensive summary and comparison of these models, readers are encouraged to refer to [El-Emam et al. \(2003\)](#).

B. Computational methods

The numerical simulation of non-Newtonian fluids in turbulent flow has garnered increasing attention in recent years, providing cost and time-efficient solutions, which has a distinct advantage over experimental methods, particularly for handling opaque fluids where conventional techniques like particle imaging velocimetry are impractical ([Rudman et al., 2004](#)). Further, most of these industries have a large network of pipelines, which cannot be experimentally observed as a whole ([Zheng et al., 2019](#)).

TABLE I. Semi-empirical models for HB fluids under turbulent flow.

Reference	Correlation	Key terms	Description
Tomita (1959)	$\frac{1}{\sqrt{f}} = \left[3.31 - \frac{(1-\phi)(\phi+3)}{2\kappa} \right] \sqrt{\frac{H(\phi, n)(1-\phi)}{2}} + 2.49 \sqrt{\frac{H(\phi, n)(1-\phi)}{2}} \ln(Re_{HB} \sqrt{f}) \quad (13)$	$Re_{HB} = 8 \frac{\rho V^{2-n}}{m} H(\phi, n) \times \left[\frac{n}{n+1} \alpha_H \cdot R(1-\phi) \frac{1+n}{n} \right]^n \quad (14)$	Tomita's expression modified for HB fluids as in Mehta <i>et al.</i> (2021), including $H(\phi, n)$ and α_H .
Dodge and Metzner (1959)	$u^+ = \frac{5.66}{(n')^{0.75}} \ln y^+ - \frac{0.4}{(n')^{1.2}} + \frac{2.458}{(n')^{0.75}} \left[1.960 + 1.255n' - 1.628n' \ln \left(3 + \frac{1}{n'} \right) \right] \quad (15)$	u^+ and y^+ are non-dimensional velocity and distance from the wall. For non-Newtonian fluids: $u^+ = \frac{u}{u_\tau}$, and, $y^+ = \frac{y^n (u_\tau)^{2-n} \rho}{m}$.	Applicable to HB fluids with n' and m' values from the Rabinowitsch-Mooney principle. Elaborated expressions can also be found in Peixinho <i>et al.</i> (2005).
Torrance (1963)	$u^+ = \frac{3.8}{n} + \frac{2.78}{n} \ln(1-\phi) + \frac{2.78}{n} \ln \left[\frac{u_\tau^{2-n} \rho y^n}{0.36n} \right] \quad (16)$	u_τ is the shear velocity [see Eq. 11], with the von Karman constant taken as 0.36n (function of the fluid's viscosity)	The expression extends the Clapp (1961) mixing length model for HB fluids.
Hanks (1978)	$Re_c = \frac{6464n}{(1+3n)^n (2+n)^{\frac{2+n}{1+n}}} \times \frac{\left[\frac{(1-\phi_c)^2}{1+3n} + \frac{2\phi_c(1-\phi_c)}{1+2n} + \frac{\phi_c^2}{1+n} \right]^{(2-n)}}{(1-\phi_c)^n} \quad (17)$	$B = \frac{22}{n} \left[1 + \frac{0.00352 \cdot He}{(1+0.000504 \cdot He)^2} \right] \quad (18)$ <p>B is a wall-effect empirical parameter.</p>	This generates $f-Re$ curves for HB fluids, similar to Moody's chart. For detailed stepwise methodology and expression for R , ϕ_c , and He refer Hanks (1978)
Thomas and Wilson (1987)			The analysis is based on the enhanced

TABLE I. (Continued.)

Reference	Correlation	Key terms	Description
	$\frac{u}{u_\tau} = \frac{V_N}{u_\tau} + 11.6(\alpha - 1) - 2.5 \ln \alpha - \Omega$ <p style="text-align: center;">V_N is the velocity of equivalent Newtonian flow.</p>	$\alpha = 2 \left(\frac{1 + \phi n}{1 + n} \right)$	viscosity due to the dissipation of micro eddies near the wall region.
			$\Omega = -2.5 \ln(1 - \phi) - 2.5\phi(1 + 0.5\phi)$
Slatter (1996)	$\frac{U}{u_\tau} = 2.5 \ln \left[\frac{R}{d_{85}} \right] + 2.5 \ln Re_\tau + 1.75$	$Re_\tau = \frac{8\rho u_\tau^2}{\tau_y + m(8u_\tau/d_x)^n}$	Based on the logarithmic velocity profile, assuming wall-adjacent particles mimic surface roughness effects.

For smooth pipes, d_x chosen by sensitivity analysis

The turbulent motions and fluctuations are governed by the unsteady three-dimensional Navier–Stokes equations coupled with the continuity equation. To numerically solve these equations, three primary methods are employed, each distinguished by the extent to which turbulence scales are resolved vs modeled: direct numerical simulation (DNS), large eddy simulation (LES), and Reynolds-averaged Navier–Stokes (RANS). Among these, RANS strikes a balance between computational efficiency and accuracy, making it the preferred method for simulating turbulent flows in industrial applications (Hanjalic, 2005; Amani et al., 2023). While RANS will be the primary focus of our discussion, we will also review recent advances in DNS and LES studies, as outlined in Sec. III B 1.

1. DNS and LES studies

DNS fully resolves turbulence by directly solving the Navier–Stokes equations across the entire range of turbulent scales, from the largest energy-containing eddies to the smallest dissipative scales (Kolmogorov scales), without turbulence modeling. One major advantage of DNS over experimental studies is the ability to investigate the sensitivity of individual parameters on flow statistics, such as average viscosity distribution and contributions of turbulent kinetic energy and viscous and non-Newtonian stresses. For instance, Singh et al. (2017b) used DNS to study the effect of yield stress on pipe flow turbulence for generalized Newtonian fluids. DNS has also been used to investigate drag reduction in the turbulent flow of visco-elastic fluids (Tsukahara et al., 2011).

Despite its accuracy, DNS remains computationally expensive. Early studies (Rudman et al., 2004; Rudman and Blackburn, 2006) focused on weakly turbulent flows with Reynolds numbers up to $Re_w \approx 8000$. These studies utilized high-order spectral element methods to capture the flow characteristics. Later, Singh et al. (2017a) extended this to $Re_w \approx 12000$, and Gavrilov and Rudyak (2016a) achieved $Re_w \approx 20000$ for PL fluids. Despite these advances, only a few studies on HB at higher Reynolds numbers exist. Industrial pipeline flows, such as those in sanitation or mining, can reach Reynolds numbers greater than $Re_w > 100000$, thus limiting DNS to transitional or weakly turbulent flows (Dash and Poelma, 2022; Basso et al., 2022).

In LES, the large, energy-containing turbulent scales of fluid motion are resolved explicitly, while the smaller, more homogeneous scales are modeled using subgrid-scale (SGS) models. This approach allows the use of relatively coarser grids compared to DNS, making LES computationally less demanding (Fröhlich and Rodi, 2002). LES has shown promise in capturing turbulent flows of non-Newtonian fluids, with notable contributions by Ohta and Miyashita (2014); Gnamboe et al. (2015), and more recently Basso et al. (2022). However, most LES studies (as discussed in detail in the next section) have either utilized standard SGS models, neglecting additional non-Newtonian correlations arising from interactions between velocity and viscosity fluctuations, or applied damping functions that fail to distinguish between viscous and non-viscous effects near walls (Amani et al., 2023; Gavrilov and Rudyak, 2016b). Additionally, many of these models focus on Newtonian-like fluids with weak shear-thinning properties or on weakly turbulent flows. Further, LES is inherently more suited to open flows (e.g., atmospheric, oceanic, or aerospace applications) rather than wall-bounded flows, as its theoretical foundations are based on the assumption of very high Reynolds numbers

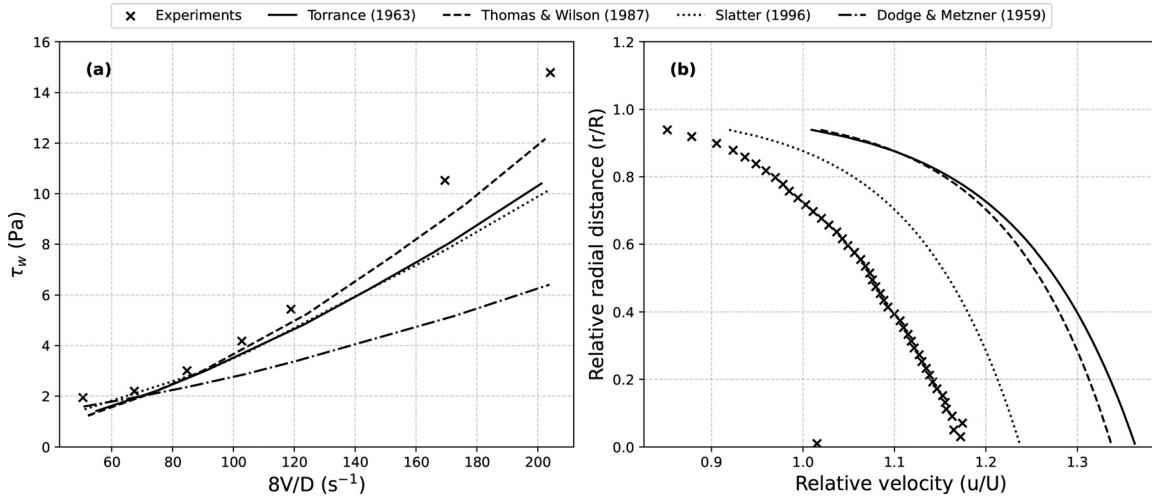


FIG. 5. Evaluation of semi-empirical models against experimental data for non-Newtonian pipe flow. (a) Wall shear stress as a function of pseudo-shear rate. Adapted from Mehta *et al.* (2021). (b) Velocity profiles across the pipe radius, compared with experimental measurements. Adapted from Yusufi *et al.* (2024), with the permission of AIP Publishing.

(Pope, 2004). For a more comprehensive discussion of employing LES in non-Newtonian fluids, one can refer to Taghvaei and Amani (2023).

2. RANS studies

RANS averages out all turbulent fluctuations over time or space, resulting in equations that describe the mean flow. This method uses a turbulence model to represent the effects of all scales of turbulence, making it computationally the least demanding but also comparatively less accurate (Alfonsi, 2011; Bouffanais, 2010; and Mehta *et al.*, 2014). Before exploring the state-of-the-art literature pertaining to RANS in detail, it is important to first understand the fundamental equations governing turbulent HB flow in a pipe. Simulating such flows requires solving the set of continuity and Navier–Stokes equations. For an incompressible flow, with gravity as the only body force, the equations can be expressed in Cartesian form as follows:

$$\frac{\partial u_i}{\partial x_i} = 0, \tag{24}$$

$$\rho \frac{\partial (u_i)}{\partial t} + \rho \frac{\partial (u_j u_i)}{\partial x_j} = - \frac{\partial p}{\partial x_i} + \frac{\partial \tau_{ij}}{\partial x_j} - \rho g. \tag{25}$$

Here, x_i ($i = 1, 2, 3$) or (x, y, z) represent the Cartesian coordinates, while u_i or (u_x, u_y, u_z) are the Cartesian components of the velocity vector \mathbf{u} . Additionally, ρ and p denote the fluid density and static pressure, respectively, while \mathbf{g} is the constant gravitational acceleration. τ_{ij} is the turbulent stress tensor and is associated with the deformation rate (or strain rate tensor, \mathbf{S}_{ij}) as follows:

$$\tau_{ij} = 2\mu \mathbf{S}_{ij}, \quad \mathbf{S}_{ij} = \frac{1}{2} \left(\frac{\partial u_j}{\partial x_i} + \frac{\partial u_i}{\partial x_j} \right), \tag{26}$$

where μ is the effective viscosity of the fluid and depends on the shear rate ($\dot{\gamma}$) as

$$\mu = \mu(\dot{\gamma}) \quad \text{and} \quad \dot{\gamma} = \sqrt{2\mathbf{S}_{ij} \cdot \mathbf{S}_{ij}}. \tag{27}$$

RANS starts with the splitting of each spatiotemporal variable in the above equations into average and fluctuating components (denoted by an overhead bar and a prime, respectively), a process known as Reynolds decomposition. For any variable θ , this can be written as

$$\theta(\mathbf{x}, t) = \bar{\theta}(\mathbf{x}) + \theta'(\mathbf{x}, t). \tag{28}$$

Further, the quantities (velocity, pressure, etc.) are ensemble averaged (averaged over many instances of the flow) to obtain a time-independent representation of the quantities, and hence the flow (Davidson, 2015)

$$\bar{\theta}(\mathbf{x}) = \lim_{T \rightarrow \infty} \frac{1}{T} \int_{t_0}^{t_0+T} \theta(\mathbf{x}, t) dt. \tag{29}$$

Now, applying Reynolds decomposition and time averaging to the above Navier–Stokes equations for Newtonian fluids, we get

$$\frac{\partial \bar{u}_i}{\partial x_i} = 0, \tag{30}$$

$$\rho \bar{u}_j \frac{\partial \bar{u}_i}{\partial x_j} = - \frac{\partial \bar{p}}{\partial x_i} + \frac{\partial}{\partial x_j} \left(\overline{\mu \dot{\gamma}_{ij}} - \rho \overline{u'_i u'_j} \right) - \rho g. \tag{31}$$

Equation (31) can be solved to obtain the ensemble average of velocity $\bar{\mathbf{u}}$ and pressure field \bar{p} , using a wide range of methods common in fluid mechanics for solving differential equations (Peric, 1985; Wilcox, 2006). However, the Reynolds stress term $(-\rho \overline{u'_i u'_j})$ remains unknown and thus requires closure. For non-Newtonian fluids with varying molecular viscosity, the decomposed and ensemble-averaged equations include additional terms related to the mean effective viscosity ($\bar{\eta}$) and its fluctuations (η'). Upon including these terms in Eq. (31), we get

$$\rho \bar{u}_j \frac{\partial \bar{u}_i}{\partial x_j} = - \frac{\partial \bar{p}}{\partial x_i} + \frac{\partial}{\partial x_j} \left(\underbrace{-\rho \overline{u'_i u'_j}}_{(1)} + \underbrace{\bar{\eta} \bar{\dot{\gamma}}_{ij}}_{(2)} + \underbrace{\overline{\eta' \dot{\gamma}'_{ij}}}_{(3)} \right) - \rho g. \tag{32}$$

Equation (32), unlike its Newtonian counterpart, includes three terms (highlighted with underbraces) that require closure: the Reynolds stress tensor, the shear-dependent viscosity, and the correlation term due to viscosity fluctuations ($\overline{\eta' \gamma'_{ij}}$). The last two correlations arise from the interaction between velocity and viscosity fluctuations, which are unknown priori and require suitable closure models. Therefore, the approximations used to close the set of RANS equations now require modifications to standard turbulence models to account for the non-linear dependency (Cszmadia and Hős, 2014; Lovato *et al.*, 2022a).

a. Wall modifications. Early efforts primarily included modifications to near-wall models, such as tweaking damping functions or, more recently, wall functions to account for rheological characteristics. For instance, Malin (1997a; 1997b) used a modified version of the Lam and Bremhorst (1981) low Reynolds number $k-\epsilon$ turbulence model to determine the friction factor (and hence pressure loss) for BP and PL fluids in smooth pipes. This approach was later extended to HB fluids (Malin, 1998). Malin proposed a damping function (f_μ) that primarily depends on the behavior index n of the fluid. The role of f_μ is to reduce the turbulent viscosity (η_t) near the wall, where the turbulence is damped as the flow becomes laminar in the viscous sub-layer. The value of f_μ obtained is then used to determine the eddy viscosity as

$$\mu_t = \frac{C_\mu f_\mu \cdot \rho \cdot k^2}{\epsilon}. \quad (33)$$

Here, k and ϵ are the turbulent kinetic energy and turbulent dissipation rate, respectively. C_μ is the model constant, which typically takes the value of 0.09 (for Newtonian fluids) and is derived from the experimental data and theoretical considerations.

Bartosik (2010) modified Malin's damping function for HB fluids by incorporating the yield stress. This analysis was based on the Wilson-Thomas hypothesis, which states that as the non-Newtonian nature of the fluids increases, the viscous sub-layer near the wall becomes thicker, suppressing the turbulence near the wall. The model was compared to known correlations, such as those by Dodge and Metzner (1959); Torrance (1963); Hanks (1978), and was found to be in good agreement. In addition to the modified damping function, Malin and Bartosik did not provide closure for shear-dependent viscosity and viscosity fluctuations and used the Newtonian RANS equations with the same model constants. While damping functions enhance the accuracy of turbulence models, particularly for low Reynolds number and near-wall regions, they have the limitation that local values typically describe these models and do not differentiate between viscous and non-viscous damping effects on the wall. An increase in molecular viscosity could be treated as proximity to the wall, inadvertently activating the damping function (Hanjalic, 2004; Gavrilov and Rudyak, 2016b).

In contrast to damping functions, another approach is to employ rheology-based wall functions, where the logarithmic law of the wall is assumed [Eq. (12)] and the model coefficients are either derived empirically or through boundary conditions such as no-slip. One significant advantage of this method is its computational efficiency, hence enabling the validation of results at high velocities (and hence high Reynolds numbers). For example, Sawko (2012) simulated turbulent PL fluids using the logarithmic law of the wall as a wall function, with model constants derived from Dodge and Metzner (1959) and Clapp (1961). Their predicted wall shear stress showed good agreement with

experimental data from Clapp, particularly at high Reynolds numbers. Similarly, Mehta *et al.* (2018a) argued that within the turbulent inner layer of the pipe, the turbulent viscosity exceeds the molecular viscosity, and hence, any fluctuations therein will also be insignificant in terms of the turbulent viscosity. Hence, Mehta used the Newtonian RANS equations but replaced the Newtonian wall function [proposed by Launder and Spalding (1974)] to include the effects of non-Newtonian viscosity in the region near the wall, where it is likely to dominate the turbulent viscosity and must be accounted for [as done by Clapp (1961) for PL fluids]

$$\frac{u}{\left(\frac{\tau_w - \tau_y}{\rho}\right)^{\frac{1}{2}}} = \frac{1}{nK} \ln \left\{ y^n \underbrace{\frac{\rho}{m} \epsilon \left(\frac{\tau_w - \tau_y}{\rho}\right)^{\frac{2-n}{2}}}_{\psi} \right\}. \quad (34)$$

ψ is a wall function based on fluid rheological parameters and is implicit in τ_w . Thus, unlike the Launder and Spalding (1974) wall function, ψ will be implemented as a specified shear boundary condition (Mehta *et al.*, 2018b). The prediction of wall shear stress and velocity profiles using these wall functions was found to be in good agreement with experimental data. The above-discussed models with their key features are summarized in Table II.

More recently, Yusufi *et al.* (2024) evaluated the performance of these wall functions over a broad range of Reynolds numbers for both wall shear stress and velocity profiles. Comparisons were made with semi-empirical and Newtonian-based models. It was observed that at high Reynolds number flows ($Re_w > 30\,000$), the modified wall function significantly improved the prediction of wall shear stress and velocity profiles, compared to Newtonian-based models (see Fig. 6). However, as the Reynolds number decreased and the flow became weakly turbulent, semi-empirical and Newtonian approaches performed better. Hence, the applicability of this approach is limited to high Reynolds number industrial flows.

Though these near-wall modifications could capture drag reductions and provide fairly accurate estimations of global flow properties, such as wall shear stress, they fail to predict local turbulence characteristics accurately (Amani *et al.*, 2023). This limitation arises because, beyond the wall modifications, these methods did not provide closure for shear-dependent viscosity and viscosity fluctuations. Instead, they relied on the Newtonian RANS equations with the same model constants. Cruz *et al.* (2004) show that even though viscosity fluctuations are quantitatively subtle, their effects on wall shear stress, velocity profiles, and turbulent kinetic energy are significant. For instance, as seen in Fig. 7(a), the fluctuating viscosity term has a negligible impact on the overall shear stress profile along the pipe radius; yet, including this term in the Navier–Stokes equations significantly improves predictions of turbulent kinetic energy [see Fig. 7(b)]. Similarly, DNS studies by Singh *et al.* (2018) demonstrate that although viscosity fluctuations contribute minimally to the mean shear stress, mean flow, and turbulent kinetic energy budgets, noticeable shear-thinning effects persist in the turbulent statistics, even at very high Reynolds numbers.

Hence, for more accurate predictions, it is crucial to incorporate closures for the non-Newtonian terms in the momentum equation [Eq. (32)] and the corresponding transport equations. This includes accounting for non-linear viscosity closures and non-Newtonian stress tensor contributions.

TABLE II. Computational methods for non-Newtonian fluids under turbulent flow.

Study	Numerical method	Description	Key features
Malin (1997a, 1998)	$k - \epsilon$ model with damping function	Adapts $k - \epsilon$ model for non-Newtonian fluids using a damping function (f_{μ}) based on behavior index (n).	Reduces turbulent viscosity near walls.
Bartosik (2010)	$k - \epsilon$ model, modified damping	Incorporates yield stress into damping functions to extend Malin's model to HB fluids.	Captures wall effects due to yield stress, validated for smooth pipes.
Pinho (2003); Cruz <i>et al.</i> (2004)	Low Reynolds number model	Introduces turbulence closures for average viscosity and non-Newtonian stress.	Models shear- and strain-rate fluctuations. Improves turbulent kinetic energy predictions.
Gavrilov and Rudyak (2016b); Durbin (1995); Hanjalic (2004)	$k - \epsilon - v^2 - f$ model	Incorporates wall-normal fluctuations (v^2) and turbulent energy redistribution (f).	Predicts turbulence anisotropy and drag reduction in PL fluids.
Lovato <i>et al.</i> (2022a)	$k - \omega$ SST model	Extends average viscosity closures to HB fluids and blends $k - \epsilon$ with $k - \omega$.	Enhanced near-wall accuracy, models anisotropy without damping functions.
Amani <i>et al.</i> (2023)	LES with recalibrated RANS constants	Integrates $k - \epsilon - v^2 - f$ with updated non-Newtonian terms and recalibrated constants.	Improved TKE and velocity predictions with LES validation.
Mehta <i>et al.</i> (2018a); Sawko (2012)	Rheology-based wall function	Employs a logarithmic law of the wall to derive non-Newtonian wall functions.	Efficient for high Reynolds numbers; validated against experimental data.
Rudman <i>et al.</i> (2004); Gavrilov and Rudyak (2016a); Singh <i>et al.</i> (2017a)	DNS	Resolves all turbulence scales, providing detailed turbulence statistics.	Highly accurate but computationally expensive; limited to weakly turbulent flows.
Ohta and Miyashita (2014); Gnamode <i>et al.</i> (2015); Basso <i>et al.</i> (2022)	LES	Resolves large scales, models smaller ones using SGS models.	Less computationally intensive than DNS; suitable for open flows.

04 March 2025 09:39:13

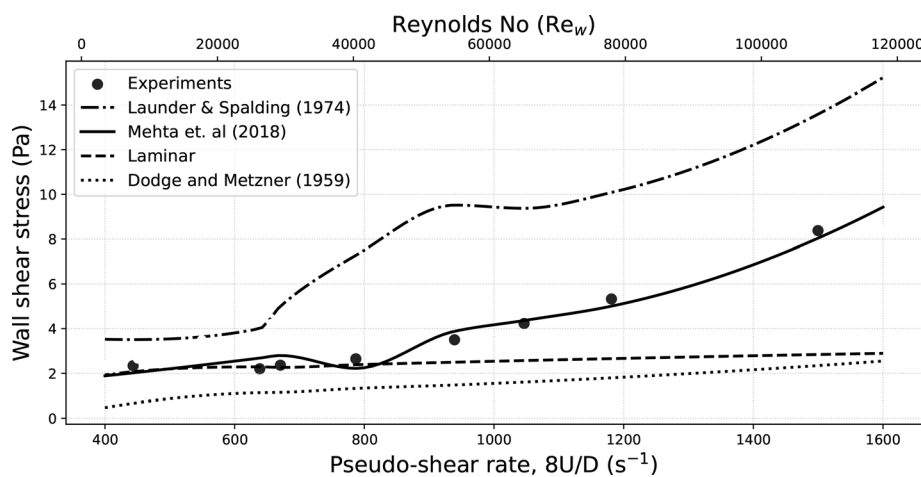


FIG. 6. Rheology-based wall function significantly enhances wall shear stress predictions at high Reynolds numbers, adapted from Yusufi *et al.* (2024), with the permission of AIP Publishing.

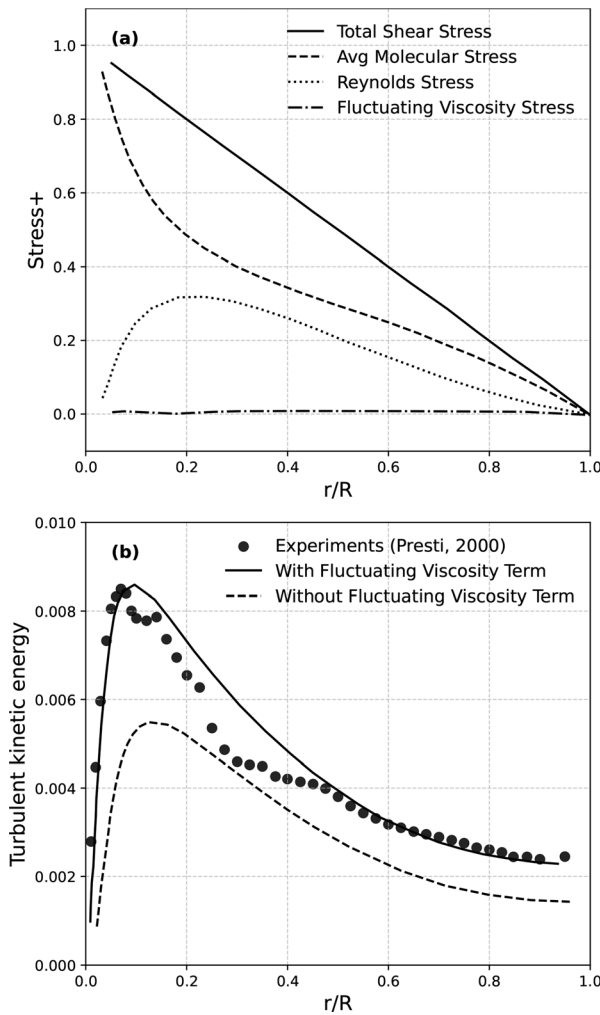


FIG. 7. Radial profiles of shear stresses and turbulent kinetic energy in non-Newtonian pipe flow, adapted from Cruz *et al.* (2004). (a) Distribution of various shear stress components across the pipe radius for $Re = 42900$. (b) Comparison of normalized turbulent kinetic energy (K/U^2) profiles with and without the fluctuating viscosity term, against experimental data from Presti (2000). Adapted with permission from Cruz *et al.*, *J. Non-Newtonian Fluid Mech.* **121** (2004) 127–141. Copyright 2004 Elsevier.

b. Models for Reynolds stresses and transport equations. The first term, Reynolds stress tensor, can be approximated using the Boussinesq hypothesis (Boussinesq, 1877), which relates Reynolds stresses to the mean rate of strain and turbulent/eddy viscosity (η_t). The approximation is expressed as

$$-\rho \overline{u'_i u'_j} = \eta_t S_{ij} - \frac{2}{3} \rho \delta_{ij} k, \quad (35)$$

where δ_{ij} is the identity tensor, and η_t is turbulent/eddy viscosity, modeled using transport equations of turbulent kinetic energy (k), turbulent dissipation rate (ϵ) and specific dissipation rate ω (Wilcox, 1988). In the context of non-Newtonian fluids, these transport equations are further augmented to include non-Newtonian contributions, such as stress

and diffusion effects caused by viscosity fluctuations. For instance, the transport equation for (k) (Gavrilov and Rudyak, 2016b) is

$$\frac{\partial(\rho k)}{\partial t} = P + D_t + D_v - \rho \epsilon + \underbrace{D_N + \Gamma_N}_{\text{Non-Newtonian}}, \quad (36)$$

here, P , D_t , D_v , $\rho \epsilon$ are turbulent production, turbulent diffusion, viscous diffusion, and viscous dissipation, respectively, while D_N , Γ_N are turbulent diffusion due to viscous fluctuations and non-Newtonian stress, respectively. Similarly, the transport equation for ϵ can be written as

$$\frac{\partial(\rho \epsilon)}{\partial t} + \frac{\partial(\rho \epsilon U_i)}{\partial x_i} = C_{\epsilon 1} \frac{\epsilon}{k} P + D_{t,\epsilon} + D_{v,\epsilon} - C_{\epsilon 2} \rho \frac{\epsilon^2}{k} + E_N, \quad (37)$$

where $C_{\epsilon 1} \frac{\epsilon}{k} P$, $D_{t,\epsilon}$, $D_{v,\epsilon}$, and $C_{\epsilon 2} \rho \frac{\epsilon^2}{k}$ represent the turbulent production, turbulent diffusion, viscous diffusion, and viscous dissipation of ϵ , respectively. The term E_N accounts for additional energy transfer and dissipation arising from non-Newtonian effects, such as viscosity fluctuations and non-Newtonian stress contributions.

State-of-the-art literature differs in its treatment of Reynolds stress, employing varying transport equations and near-wall modeling strategies. For instance, Pinho (2003) developed a low Reynolds number formulation based on the $k - \epsilon$ model of Nagano and Hishida (1987), incorporating a turbulence closure for non-Newtonian correlations and a model for average viscosity that accounts for fluctuations in shear and strain rates. In a companion study, Cruz and Pinho (2003) validated the model against Malin's and Dodge & Metzner's correlations, and it showed good agreement with the experimental data of Escudier and Presti (1996), thus laying the groundwork for future advancements in non-Newtonian fluid turbulence modeling. Cruz *et al.* (2004) further improved the model by including cross-correlation terms between fluctuating viscosity and deformation rate tensors. The model was subsequently extended to finitely extensible nonlinear elastic (FENE-P) fluids using Peterlin's approximation (Pinho *et al.*, 2008) and later adapted to better predict drag reduction levels through a $k - \omega$ model (Resende *et al.*, 2013). Despite these advancements, the model assumes isotropic turbulence, which may hold for Newtonian fluids but not for non-Newtonian fluids that exhibit significant anisotropy (Gavrilov and Rudyak, 2016b). This anisotropic behavior under turbulent flow has also been observed in various experiments such as Güzel *et al.* (2009) and Mitishita *et al.* (2021). Therefore, the applicability of such models for highly non-Newtonian fluids at high Reynolds numbers is yet to be established and seems unworkable until proven otherwise.

Gavrilov and Rudyak (2016b) sought to address these limitations for PL fluids by adopting the approach of Durbin (1995), which accounts for the non-viscous damping effects of walls through a turbulent energy redistribution mechanism. They employed a four-equation $k - \epsilon - v^2 - f$ turbulence model, based on Hanjalic (2004), incorporating an additional transport equation for v^2 , which depends on the wall-normal velocity distribution and turbulence kinetic energy, and f , an elliptical relaxation function representing turbulent energy redistribution. The closure for non-Newtonian stress was derived under the assumption that viscosity fluctuations (η') are negligible compared to the average viscosity (η), i.e., $\eta' \ll \eta$.

This model effectively predicted wall-normal fluctuations and intrinsic near-wall damping effects without resorting to *ad hoc*

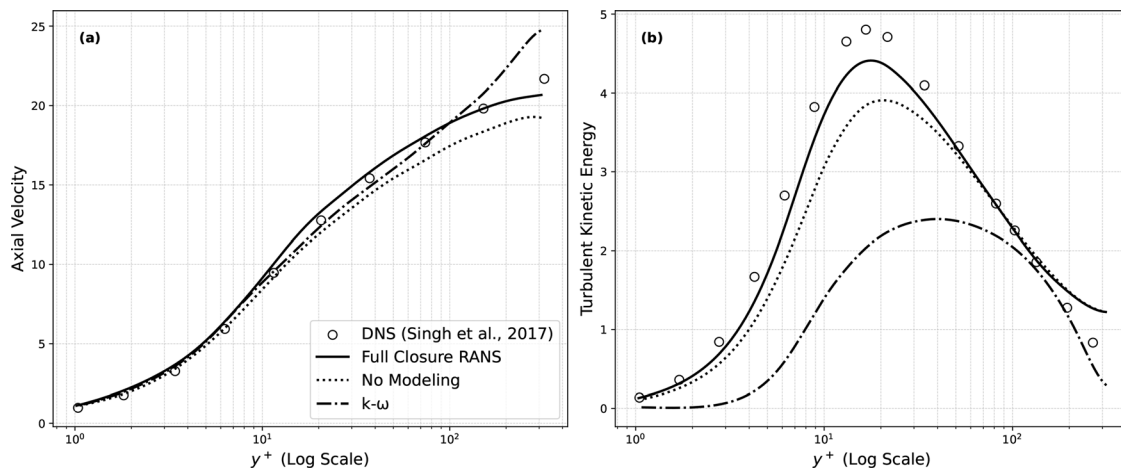


FIG. 8. Comparison of normalized mean velocity (a) and turbulent kinetic energy (b) profiles predicted by the RANS models (with and without non-Newtonian terms) and the $k - \omega$ Shear-Stress Transport (SST) model against DNS results from Singh *et al.* (2017a). Reproduced with permission from Amani *et al.*, Int. J. Heat Fluid Flow **99**, 2023. Copyright 2023 Elsevier.

damping functions, as validated against LES results in Amani *et al.* (2023). It also enhanced drag reduction predictions in turbulent flows of non-Newtonian fluids. Validation against Rudman's DNS data up to $Re_w = 5500$ showed good agreement. However, as noted by Charles *et al.* (2024), this does not necessarily indicate a fully developed turbulent flow. Further, at higher Reynolds numbers, the contribution of turbulent viscosity to dissipation surpasses that of molecular viscosity, suggesting that the assumption $\eta' \ll \eta$ may not always hold true [see Fig. 7(b) and Mehta *et al.* (2018a)].

Lovato *et al.* (2022a) extended Gavrilov's approach to HB fluids ($n = 0.8$, and, $\tau_y/\tau_w = 0.1$) by incorporating anisotropic turbulence using the $k - \omega$ SST model developed by Menter (1994). Being a blend of the $k - \epsilon$ and $k - \omega$ models, the SST model combines the insensitivity to free-stream parameters of the $k - \epsilon$ model with the near-wall accuracy of the $k - \omega$ model without requiring damping functions (Menter *et al.*, 2003). The model's predictions for friction factor and velocity profiles showed good agreement with both DNS data and correlations for PL and BP fluids. While the model is robust and validated for accurately predicting the complex flow behaviors of PL fluids, it requires further validation for highly non-Newtonian HB fluids (with $n < 0.5$ and high yield stress) and under more turbulent conditions.

Recently, Amani *et al.* (2023) highlighted limitations in the $k - \omega$ and $k - \omega$ SST models for non-Newtonian flows. While these models are robust for wall-bounded turbulent flows in Newtonian fluids, they struggle to predict local turbulence characteristics and anisotropy in non-Newtonian fluids due to their reliance on isotropic eddy viscosity and lack of wall-normal fluctuation variables. Specifically, the $k - \omega$ framework underpredicted turbulent kinetic energy (TKE) and near-wall anisotropy in drag-reducing flows (see Fig. 8). Building on Gavrilov and Rudyak (2016b) methodology, Amani recalibrated constants ($C_N = 0.8$, $C_{eN} = 1.0$), achieving significant accuracy gains in velocity predictions (from 11.8% to 6.6%) and TKE (from 3.7% to 4%). However, the study highlighted the sensitivity of RANS predictions to model constants, suggesting potential limitations for high-Reynolds-number flows.

c. Models for average viscosity. Gavrilov and Rudyak (2016b) proposed a model for the average viscosity [second term in Eq. (32)], assuming that the average viscosity is a function of the mean shear rate, as expressed in Eq. (27). The mean squared shear rate, derived from the decomposition of strain rate fluctuations and the energy dissipation rate, is given as

$$\dot{\gamma}^2 = 2S_{ij}S_{ij} + \frac{\rho\epsilon}{\eta}. \quad (38)$$

Here, the first term represents contributions from the mean strain rate tensor, while the second term accounts for turbulence dissipation effects. Since both Eqs. (27) and (38) are implicit in μ , the average viscosity must be solved iteratively or numerically. For high Reynolds number flows, Pinho (2003) simplified the model, approximating the viscosity as a function of dissipation rate alone, highlighting the dominant role of dissipation in governing viscosity in turbulent regimes. Pinho (2003) emphasized the statistical variability of dissipation due to turbulence intermittency, arguing that the dissipation rate (ϵ) follows a lognormal distribution at high Reynolds numbers. They proposed a semi-empirical model for the average viscosity, incorporating both the variance of $\ln \epsilon$ and the influence of turbulence length scales (energy-containing large eddies and dissipative Kolmogorov scales). This correction captures the effects of rare but extreme dissipation events on the average viscosity, making the model particularly suitable for highly intermittent flows such as those with drag-reducing additives or viscoelastic fluids.

d. Models for fluctuating viscosity stress tensor. The non-Newtonian Fluctuating Viscosity Stress Tensor [third term in the underbrace in Eq. (32)] arises due to the correlation between viscosity and strain-rate fluctuations. Though quantitatively small compared to the average molecular or Reynolds stresses, it has been shown to significantly improve turbulence predictions when included, as demonstrated in several numerical studies (Amani *et al.*, 2023; Singh *et al.*,

2018; and Cruz *et al.*, 2004). Hence, it requires appropriate closure. Gavrilov and Rudyak (2016b) attempted to model these stresses, assuming small viscosity fluctuations ($\eta'/\eta \ll 1$) and linearizing the dependence of η' on the shear rate

$$\eta' \propto (n-1) \frac{\eta}{\dot{\gamma}^2} S_{ij} \cdot S'_{ij}. \quad (39)$$

Here, the squared shear rate ($\dot{\gamma}^2$) is given by Eq. (38), and it is implicit in η , requiring numerical solutions such as the Newton-Raphson method (Amani *et al.*, 2023).

Cruz *et al.* (2004) assumed that fluctuations in viscosity (η') have dissipative effects and models η' as being proportional to fluctuations in the dissipation rate (ϵ'). This assumption aligns with the understanding that shear-thinning influences turbulence dissipation. Consequently, the non-Newtonian stress term ($2\eta'\dot{\gamma}'_{ij}$) is modeled to behave similarly to damping functions commonly used in turbulence models, particularly near the wall where turbulence is suppressed

$$\eta' \propto m(\dot{\gamma}')^{n-1}. \quad (40)$$

To achieve this, the non-Newtonian stress term is semi-empirically derived as a function of damping constants (C_μ, f_μ), turbulence length scales (L_c), and turbulent flow properties such as turbulent kinetic energy (k) and its dissipation rate (ϵ). The model ensures that this stress vanishes in the Newtonian limit, reflecting the absence of viscosity fluctuations. Additionally, it incorporates rheological parameters (n, m) to account for the shear-thinning behavior of viscoelastic fluids, which play a critical role in drag reduction phenomena.

Though numerous numerical and experimental studies have highlighted the importance of incorporating non-Newtonian contributions (Cruz *et al.*, 2004; Güzel *et al.*, 2009; J. Singh, 2016; and Amani *et al.*, 2023). For instance, Amani *et al.* (2023) demonstrated that neglecting non-Newtonian terms in the momentum and transport equations can lead to underestimations of up to 11% in velocity profiles and 18.8% in turbulent kinetic energy profiles (Fig. 8). Despite these findings, the current state-of-the-art literature methodologies are based on three key assumptions requiring further validation: (1) the simplification of the coupling between molecular viscosity and turbulent strain rates, often treated linearly or through empirical functions, which overlooks the complex shear rate dependencies of non-Newtonian fluids; (2) the neglect or approximation of higher-order nonlinear terms in stress closures, limiting accuracy in capturing phenomena like drag reduction and turbulence suppression; and (3) the assumption of isotropic turbulence, which fails to account for the significant anisotropy characteristic of non-Newtonian flows, such as dominant streamwise fluctuations.

Also, the current literature lacks comprehensive studies comparing the various approaches to modeling Reynolds stress, average viscosity, and fluctuating viscosity stress tensors. One reason for this gap is that while such models have proven highly accurate, especially for capturing local turbulent properties, they are often complex to implement and computationally expensive. Moreover, many of these models are tuned using default Newtonian constants, which limit their applicability and accuracy under highly non-Newtonian conditions, necessitating further refinement and development.

In industrially relevant high-turbulence scenarios, simpler approaches—such as rheology-based wall functions or semi-empirical models (formulated decades ago)—continue to be widely used.

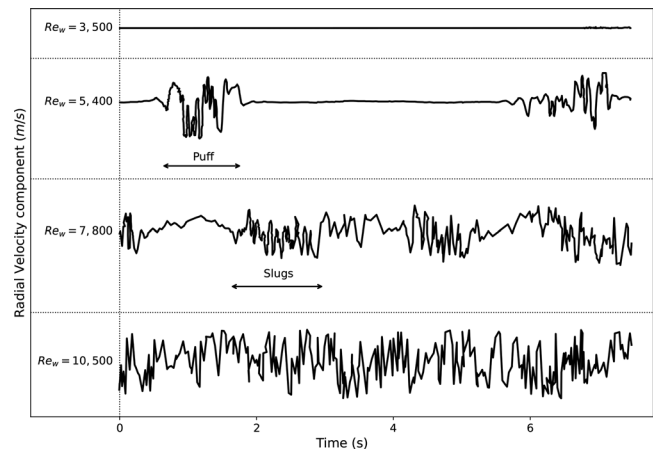


FIG. 9. Observing transition through the ultrasound velocimetry data. Adapted from Krishnan Thota Radhakrishnan *et al.* (2021), under the terms of the Creative Commons Attribution-Non Commercial-No Derivatives License (<http://creativecommons.org/licenses/by-nc-nd/4.0/>), which permits noncommercial reuse, distribution, and reproduction in any medium, provided the original work is properly cited and not altered or transformed in any way.

However, as discussed previously, these approaches rely on significant assumptions and simplifications. While they perform reasonably well under high turbulent conditions, they often underperform at relatively low Reynolds numbers (despite turbulent conditions) or under extreme non-Newtonian behaviors. Further, the lack of a clearly defined operational envelope makes it difficult to determine the appropriate model for a specific Reynolds number or flow condition. Addressing these challenges requires more experimental data, further development of robust modeling frameworks, and detailed comparison and validation studies to guide practical applications.

IV. LAMINAR-TURBULENT TRANSITION IN HB FLUIDS

Previous studies on Newtonian (Wynanski and Champagne, 1973; Wynanski *et al.*, 1975; and Nishi *et al.*, 2008) and non-Newtonian fluids (Draad *et al.*, 1998; Güzel *et al.*, 2009) have shown that the transition to turbulence in pipe flow is not a singular event but a gradual process characterized by the formation of intermittent flow structures. These structures, called puffs and slugs (see Fig. 9), evolve due to disturbances within the flow and are often accompanied by temporal variations in local velocities (Nishi *et al.*, 2008). In Newtonian fluids, puffs typically occur at lower Reynolds numbers ($Re < 2700$), while slugs are more prevalent at higher Re ($Re > 3000$). Recent investigations on HB fluids (Krishnan Thota Radhakrishnan *et al.*, 2021; Charles *et al.*, 2024) have corroborated the existence of intermittent flow structures during the transition process. However, these studies have revealed a delay in the onset of puffs and slugs compared to Newtonian fluids. For instance, Krishnan Thota Radhakrishnan *et al.* (2021) observed puff formation at around $Re_w \approx 5400$ and slug formation at $Re_w \approx 10500$ (refer to Fig. 9), while Charles *et al.* (2024) reported a range of $Re_w \approx 3310 - 6260$ for the appearance of these structures.

As the transition regime is characterized by highly non-linear momentum transfer and the formation of time-dependent intermittent structures, such as eddies and localized turbulent patches, models

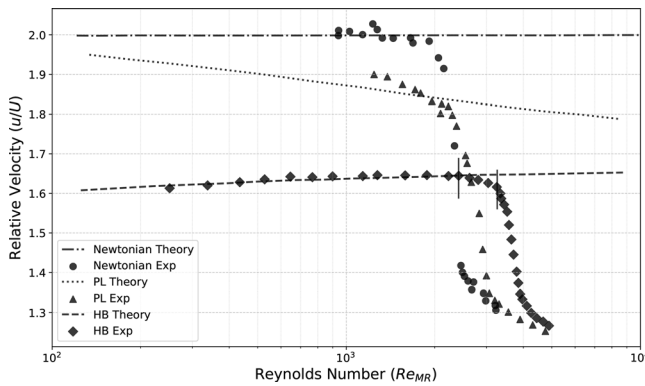


FIG. 10. Transition from laminar to turbulent flow for Newtonian, PL, and HB fluids. The semi-logarithmic plot displays the centerline velocity ratio (u/U) as a function of the Reynolds number (Re_{MR}). Dotted and dashed lines represent theoretical predictions for laminar flow, while markers indicate experimental data: circles for Newtonian fluids, triangles for PL fluids, and diamonds for HB fluids. Black solid lines delineate the transition regions. Adapted with permission from Peixinho *et al.*, *J. Non-Newtonian Fluid Mech.* **128**, 172–184 (2005). Copyright 2005 Elsevier.

developed for laminar or turbulent flows often fail to provide accurate predictions in the transition zone (Erge *et al.*, 2015; Draad *et al.*, 1998). Figure 10 illustrates how the centerline velocity of both Newtonian and non-Newtonian fluids, such as PL and HB fluids, significantly drops beyond a critical point—a change that theoretical models often fail to capture accurately. Also, unlike laminar and turbulent flows, which can be approximated by models with certain assumptions, the characteristics of transition complicate the modeling process even for Newtonian fluids. For non-Newtonian HB fluids, the problem is further exacerbated as both shear-thinning properties and yield stress contribute to stabilizing the flow, delaying the onset of turbulence even further. This is evident from the experimental observation of Charles *et al.* (2024) and Krishnan Thota Radhakrishnan *et al.* (2021), and could also be observed from Figure 10 that the deviation from theoretical laminar behavior is delayed for PL fluids compared to Newtonian fluids, with an even further delay noted for HB fluids when compared to PL fluids. Güzel *et al.* (2009) concluded that for HB fluids, the transition begins when local stresses exceed the yield stress, breaking the plug region and triggering localized disturbances. These disturbances eventually grow and merge, forming large-scale turbulence, and the plug region [refer to Fig. 3] breaks down at the onset of transition, leading to turbulence.

Along the same lines, other studies, such as Reed and Pilehvari (1993), investigated the role of the Hedstrom number [Eq. (41)]—a dimensionless parameter and measure of yield stress. Their findings showed that the presence of yield stress not only delayed the transition but also widened the range of Reynolds numbers over which the transition occurred. For example, in BP fluids, the transition to fully turbulent flow was delayed until a Reynolds number (Re_w) of approximately 100 000 when the Hedstrom number exceeded 500 000. This demonstrates the significant role of yield stress in stabilizing flow, delaying turbulence, and widening the transition zone. However, some studies have reported contrasting behavior. For instance, Erge *et al.* (2015) found that while the transition in HB fluids is highly dependent on the fluid's rheological properties and pipe diameter, fluids with more

pronounced non-Newtonian characteristics (higher yield stress and lower behavior index) tend to transition to turbulence earlier than fluids with weaker non-Newtonian properties.

$$He = \frac{\rho D^2 \tau_y}{\mu^2}. \quad (41)$$

Consequently, due to this complexity, researchers and engineers often prefer to avoid operating in the transition zone, instead aiming for fully laminar or fully turbulent conditions. Consequently, understanding the transition zone becomes essential for defining an operational envelope for analytical equations related to laminar flow. In some cases, engineers are interested in knowing what conditions will trigger turbulence and modifying existing systems that may be operating in laminar flow. In essence, the problem reduces to theoretically predicting the onset of transition (called a critical condition) and subsequently determining critical velocity or critical Reynolds number, or their equivalents for non-Newtonian fluids (Dash, 2022). For Newtonian fluids, the transition typically occurs at a Reynolds number of around 2100, as defined by the classical Reynolds number (Jackson and Launder, 2007; Chhabra and Richardson, 2008a).

However, as briefly discussed in Sec. II B, the available definitions of the Reynolds number for non-Newtonian fluids are inconsistent both experimentally and numerically in capturing the onset of turbulence (Güzel *et al.*, 2009; Charles *et al.*, 2024). Despite this, several models have been proposed to predict the critical conditions for this transition. This section has focused on the theoretical and empirical models available in the literature; experimental studies and their findings can be found in the preceding section. These models generally fall into two categories: stability parameter-based models and Reynolds number-based models (Erge *et al.*, 2015; Krishnan Thota Radhakrishnan *et al.*, 2021).

A. Stability-based transition models

Stability-based models predict flow stability and the onset of turbulence by assessing the balance between stabilizing and destabilizing forces using stability parameters. For instance, Ryan and Johnson (1959) proposed a local stability parameter (Z_{RJ}) to determine the onset of transition based on the energy dissipation of disturbances, represented as shear stresses. At this critical point, Z_{RJ} takes a value of 808, which was derived by considering the critical Reynolds no. for Newtonian fluids to be 2100 [see Eq. (42)]. It was proposed that the method can be used for non-Newtonian fluids as well since the stability parameter (Z_{RJ}) does not depend on the fluid properties.

Later, Hanks (Hanks, 1963, 1969; Hanks and Dadia, 1971; and Hanks and Ricks, 1974) extended Ryan and Johnson's work to non-Newtonian fluids using the concept of angular momentum transfer. The proposed stability parameter (K) represents a ratio of the rate of change of angular momentum of the deforming fluid to its rate of momentum loss by frictional drag [Eq. (43)]. At transition, the fluid element is seen to become unstable, and the formation of eddies starts due to the nonlinearity of the momentum transfer process. At this stage, the maximum value attained by the stability parameter (K_{max}) is 404, corresponding to the critical Reynolds number (Newtonian's) of 2100. It was assumed that this Z_{max} would be the same for all fluids at the critical point.

TABLE III. Stability and Reynolds number-based transition models.

Study	Method	Model	Transition criteria
Ryan and Johnson (1959)	Stability based	$Z_{RI} = \frac{r\rho v_z}{\tau_w} \frac{\partial v_z}{\partial y}$ (42)	Transition predicted when $\frac{\partial Z_{RI}}{\partial y} = 0$.
Hanks (1969)	Stability based	$K = \sqrt{\frac{1}{27} Re}$ (43)	Transition at $K_{max} = 404$.
Mishra and Tripathi (1971)	Stability based	$X = \frac{\rho U^2}{\alpha \tau_w} = \frac{2}{\alpha f} = \frac{Re}{8\alpha}$ (44)	Occurs where the mean velocity rate of change is maximal.
Metzner and Reed (1955)	Reynolds number based	$Re_{MR} = \frac{8\rho U^2}{m' \left(\frac{8U}{D}\right)^n}$ (45)	Transition when $f \approx 0.0076$.
Torrance (1963)	Reynolds number based	$Re_{Tr} = \frac{8\rho U^2}{m \left[\frac{8U}{D}\right]^n}$ (46)	Occurs within Newtonian transition range.
Slatter (1995)	Reynolds number based	$Re_{ST} = \frac{8\rho U_{ann}^2}{\tau_y + K(8U_{ann}/D_{shear})^n}$ (47)	Transition at $Re_{ST} = 2100$.

Mishra and Tripathi (1971) postulated that the transition from laminar to turbulent flow occurs in steps: first, the formation of 2-D waves, which then change to 3 D waves, then turbulent spots begin to appear, and finally, in fully turbulent flow, these spots propagate to the entire cross section. The formation of these turbulent spots is a local phenomenon and coincides with the maximum rate of change of the kinetic energy (of the mean velocity). This can be considered as the critical condition for transition. Based on the assumption that at the onset of turbulence, the ratio of average kinetic energy per unit volume to wall shear stress is the same for all the purely viscous non-Newtonian fluids, a stability parameter (X) was proposed [Eq. (44)]. The aforementioned models and their correlation are summarized in Table III.

Krishnan Thota Radhakrishnan et al. (2021) performed a comparative analysis of stability-based methods and found that the Hanks method performed slightly better for HB fluids. They argued that these methods are very similar in implementation and differ primarily in their development. The Hanks model, being well-documented for HB fluids, is easier to implement compared to other methods. Stability-based methods assume that the stability parameter takes a critical value

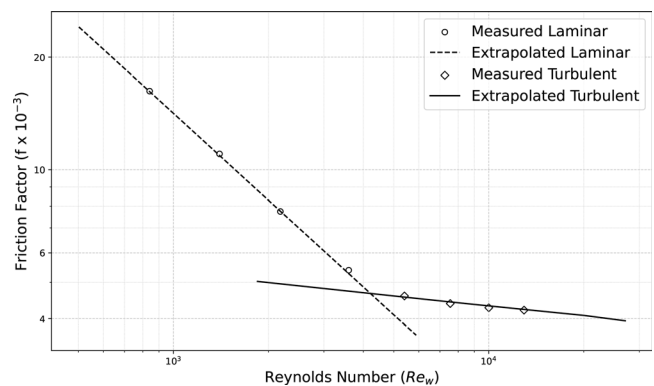


FIG. 11. Determining the critical Reynolds number (Re_{ST}) using the Intersection method. Adapted from Krishnan Thota Radhakrishnan et al. (2021), under the terms of the Creative Commons Attribution-NonCommercial-NoDerivatives License (<http://creativecommons.org/licenses/by-nc-nd/4.0/>), which permits noncommercial reuse, distribution, and reproduction in any medium, provided the original work is properly cited and not altered or transformed in any way.

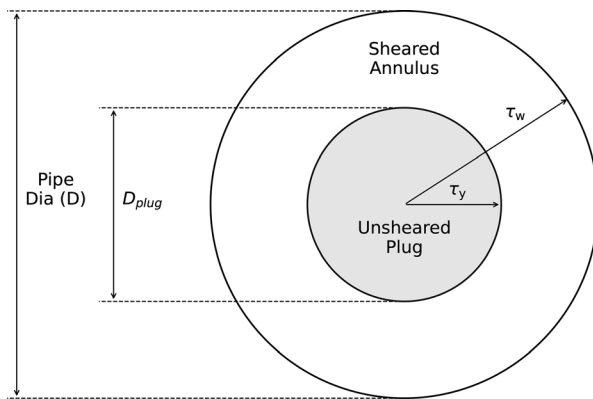


FIG. 12. Slatter's unsheared plug geometry.

at the transition point, which is the same for both Newtonian and non-Newtonian fluids. However, [Slatter \(1995\)](#) found that Z_{max} shows an increasing trend with an increase in Hedstrom number. A similar observation was made by [Güçüyener et al. \(1996\)](#), who found that the stability parameters are sensitive to yield stress.

B. Reynolds number-based transition models

Reynolds number-based models attempt to extend the classical Reynolds number framework to non-Newtonian fluids by incorporating additional parameters such as yield stress and shear-thinning effects. One such method is the intersection method proposed by [Hedström \(1952\)](#), which predicts the transition by identifying the intersection of extended laminar and turbulent friction factor curves (see [Fig. 11](#)). While this method offers a simple and straightforward approach to estimating the transition, its accuracy is largely dependent on the choice of the turbulent model employed.

[Metzner and Reed \(1955\)](#) analyzed a series of pipe flow experimental data sets for non-Newtonian fluids to identify the critical Reynolds number marking the onset of turbulence, at which flow begins to deviate from laminar behavior. Instead of directly evaluating the critical Reynolds number, the critical Fanning friction factor (f) is considered. It was proposed that when f falls to 0.0076 or lower, or when the Reynolds number [discussed in the previous section, [Eq. \(7\)](#)] is in the range of 2000–2500, both Newtonian and non-Newtonian fluids enter the transition range. Subsequent studies by [Torrance \(1963\)](#) and [Clapp \(1961\)](#) proposed similar forms of the Reynolds number for non-Newtonian HB fluids [see [Eq. \(46\)](#)]. However, these definitions assume that the transition occurs within a range comparable to that of Newtonian fluids, which is contradicted by various experimental studies [e.g., [Güzel et al. \(2009\)](#) and the recent work by [Charles et al. \(2024\)](#)] indicating that shear-thinning behavior delays transition.

Another consideration is the role of yield stress, which has been ignored in the previously mentioned definitions. [Slatter \(1995\)](#) argued that to account for the full viscous stress, yield stress has to be considered in the analysis. They proposed a non-Newtonian version of the Reynolds number for HB fluids, which can be used to determine the laminar-turbulent transition. This formulation is based on the existence of a solid unsheared plug concentric with the pipe axis for fluids with yield stress [see [Fig. 12](#) and [Eq. \(47\)](#)], suggesting that only the

sheared annulus should be considered as the fluidic part where turbulence develops.

Comparing their model with other Reynolds number-based correlations [also see [Eshtiaghi et al. \(2012\)](#)], Slatter found that their model performed best in determining the transition, while other models tended to underpredict it. They attributed this discrepancy to the fact that other models overlooked the unsheared plug, which constitutes a significant portion of the pipe in yield stress fluids. However, [Güzel et al. \(2009\)](#) observed in their experimental investigation that both PL and HB fluids behaved similarly during transitional flow, raising questions about the effect of the plug. They suggested that during the transition, the plug thins to the degree that Reynolds stresses become sufficient to disrupt it. Recent experimental work by [Charles et al. \(2024\)](#) also indicated that the presence of yield stress and shear thinning delayed the transition; they believe that it is because of yield stress. Nonetheless, studies that independently investigate the effects of shear-thinning and yield stress are still lacking, largely due to the difficulty in finding materials that exhibit these properties in isolation. Consequently, there is uncertainty over how the transition occurs in these fluids, the role of the plug, and how it behaves during the transition.

In another study, [Van den Heever et al. \(2014\)](#) conducted a comparative analysis of these Reynolds number-based parameters. Their study revealed that these methods are heavily dependent on the fitted rheological model, with errors in transitional velocity prediction ranging from 2.5% to 31%. Such discrepancies complicate the establishment of a clear preference for any particular method. This underscores the need for future research to focus on refining these models and improving experimental techniques to capture transitional behaviors more accurately, especially for industrial applications where non-Newtonian fluids are commonly used.

V. EXPERIMENTAL DEVELOPMENTS

The early developments in the experimental research of non-Newtonian fluids include the work of [Metzner and Reed \(1955\)](#), who compiled data from multiple sources on the flow of 16 different non-Newtonian fluids, including clay suspensions, polymeric solutions, and slurries of cement rock and lime characterized as pseudoplastic, dilatant and BP fluids. The data were used to establish a relationship between the friction factor and the generalized Reynolds number for non-Newtonian fluids under laminar flow ([Sec. II B](#)) and focus on defining the transition from laminar to turbulent flow ([Sec. IV B](#)). [Dodge and Metzner \(1959\)](#) conducted experiments on polymeric gels and solid-liquid suspensions, with flow behavior (n) indices ranging from 0.3 to 1.0, through smooth pipes of varying diameters (1.27–5.08 cm). They measured pressure drops across different sections of the pipes at various flow rates under turbulent conditions, with Reynolds numbers (Re_{MR}) reaching up to 36 000. These measurements were used to propose a friction factor-Reynolds number correlation and theoretical expression for the velocity profile in turbulent non-Newtonian fluids [[Eq. \(15\)](#)]. However, these developments are limited to polymeric solutions and suspensions, which, unlike HB fluids, do not require initial yield stress to flow.

[Slatter \(1996\)](#) conducted an extensive experimental campaign on slurries with a wide range of volumetric concentrations (2% to 37%), which behave rheologically as HB fluids. The pipeline test loop included sections with diameters ranging from 6 to 200 mm to measure flow rate and corresponding wall shear stress. Based on these

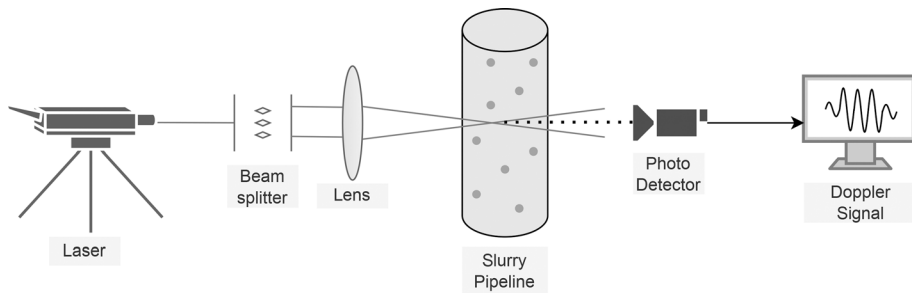


FIG. 13. Laser Doppler velocimetry (LDV) system schematics.

experiments, Slatter proposed critical Reynolds numbers and logarithmic velocity profile expressions for both smooth and rough pipes (as discussed in the previous sections). His analysis, however, was solely based on wall shear stress measurements. In contrast, velocity profiles offer a more detailed and sensitive indicator of a fluid's rheology (Park *et al.*, 1989b).

Studies measuring velocity profiles and turbulence characteristics of HB fluids are limited, primarily due to the opaque nature of these suspensions and high particle concentrations, which present significant challenges for non-intrusive velocity profile measurements (Hogendoorn *et al.*, 2021). These challenges are further compounded under turbulent flow conditions, and the current experimental techniques often fail to meet the spatial and time resolution requirements to study the near-wall region. Techniques like hot-wire anemometry work well away from the wall but have limitations close to it due to their invasive nature and the disturbance they cause to the flow (Durst *et al.*, 1995).

Non-intrusive flow velocimetry techniques can be broadly categorized into (1) optical methods, such as Particle Image Velocimetry (PIV) and Laser Doppler Velocimetry (LDV), and (2) acoustic methods, such as Ultrasound Doppler Velocimetry (UDV). Other advanced techniques, such as X-ray Imaging, Magnetic Resonance Imaging (MRI), and Electrical Capacitance Tomography (ECT), face limitations regarding resolution, complexity, cost, and radiation exposure. Therefore, these methods are not discussed here due to their limited applicability in this context. For a more comprehensive overview of these methods, readers are referred to Poelma (2020).

A. Optical techniques

Optical methods such as PIV and LDV are well-established and widely used in experimental fluid mechanics, offering high spatial and temporal resolution in capturing detailed velocity fields and turbulence characteristics (Wiederseiner *et al.*, 2011). Both techniques rely on the scattering of laser light by moving particles, which are subsequently converted into velocity information. However, the methods differ in their measurement approach: LDV is a point-based technique that offers velocity measurements at specific locations, whereas PIV delivers global, instantaneous velocity profiles over an entire field (Silva, 2022). A schematic of the LDV measurement setup is illustrated in Fig. 13. For the non-Newtonian fluids, Park *et al.* (1989a) were the first to experimentally measure velocity profiles in turbulent HB fluids. They investigated the flow characteristics of an optically transparent HB slurry using Laser Doppler Velocimetry (LDV) with refractive index matching. They found that while the mean velocity profile in turbulent flow followed the $1/7$ th power law typical of Newtonian fluids, the

tangential turbulence intensity was significantly higher near the wall. Additionally, the transition to turbulence occurred over a narrower velocity range with lower peak turbulence intensity compared to Newtonian fluids, highlighting distinct differences in flow behavior under these conditions.

Escudier and Presti (1996) studied the pipe flow of a thixotropic Laponite solution, modeled as an HB fluid with a yield stress of 4.4 Pa, over Reynolds numbers (Re_w) from 274 to 49 000. Using laser Doppler velocimetry (LDV), they found that at low Reynolds numbers (< 1300), the velocity profile was symmetric and matched the HB model. As Reynolds numbers increased (1300–3000), the profiles became asymmetric, indicating instability, but returned to symmetry at higher Reynolds numbers. In turbulent flow, the Laponite solution exhibited drag reduction, with reduced tangential and radial turbulence intensities. The study also noted that the effective wall viscosity was lower than expected, reflecting the thixotropic nature of the fluid.

Peixinho *et al.* (2005) experimentally investigated the laminar, transitional, and turbulent flows of a 0.2% Carbopol solution (rheologically behaves as HB) in a cylindrical pipe, comparing it with a shear-thinning fluid (2% CMC solution) and a Newtonian fluid (glucose syrup). Their findings indicate that both the yield stress and shear-thinning effects delayed the transition to turbulence. In turbulent flow,

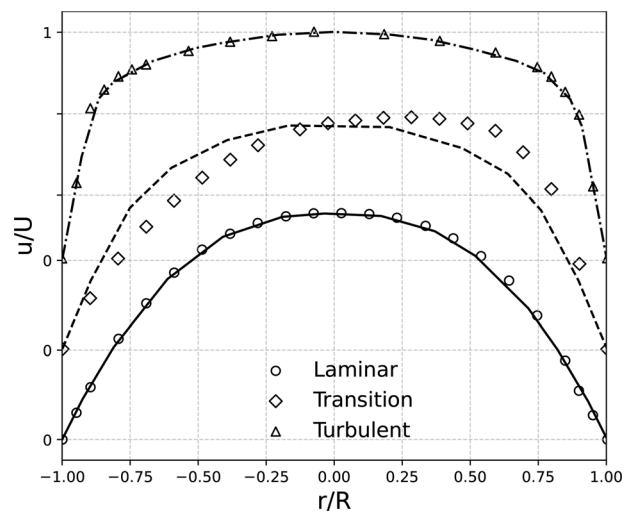


FIG. 14. Asymmetric mean velocity profiles in pipe flow during the transition regime, as observed in Güzel *et al.* (2009), Escudier *et al.* (1999), and Peixinho *et al.* (2005). Adapted with permission from Güzel *et al.*, *J. Fluid Mech.* **627**, 97–128 (2009). Copyright 2009 Cambridge University Press.

TABLE IV. Summary of experimental studies on non-Newtonian fluid flow.

Study	Measurement technique	Fluid properties	Flow conditions	Key findings
Park <i>et al.</i> (1989a)	LDV	HB, $\tau_y = 10$ Pa, $n = 0.63$, $m = 0.167$ Pa·s ^{<i>n</i>}	Transitional, Turbulent, $Re_w = 225$ – $27\,800$	Higher turbulence near walls; mean velocity follows 1/7th power law; narrow turbulence transition.
Escudier and Presti (1996)	LDV	Thixotropic HB, $\tau_y = 4.4$ Pa	Laminar ($Re_w < 1300$), Transitional, Weakly Turbulent	Asymmetric velocity profiles in transition; drag reduction and lower effective viscosity at walls in turbulent flow.
Peixinho <i>et al.</i> (2005)	LDV	Newtonian, PL, HB (Carbopol), $\tau_y = 7.2$ Pa, $m = 4.3$ Pa·s ^{<i>n</i>} , $n = 0.47$	Laminar, Transitional, Turbulent, $Re_w \leq 3300$	Delayed transition due to yield stress; observed drag reduction and higher near-wall turbulence intensity.
Güzel <i>et al.</i> (2009)	LDV, high-speed Imaging	Newtonian, PL, HB	Transitional	Profile asymmetry; intermittent turbulent structures such as puffs and slugs observed in transition phase.
Charles <i>et al.</i> (2024)	High-speed Camera	HB (Carbopol)	Pre-transition, Transitional	Detected pre-transition asymmetry; delayed turbulence onset due to yield stress-shear thinning interactions.
Benslimane <i>et al.</i> (2016)	UDV	HB (Bentonite, 3.5–8% conc.)	Laminar, Transitional, Turbulent	Validated laminar profile; asymmetric flow in transition; turbulent profile aligned with correlation by Dodge and Metzner (1959).
Krishnan Thota Radhakrishnan <i>et al.</i> (2021)	UIV	PL, HB (Kaolin, up to 20% w/w)	Laminar, Transitional, Turbulent	Puffs and slugs mapped; detailed characterization of flow during transition with UIV.
Dash (2022)	UIV	HB (Kaolin, 21% w/w, $\tau_y = 0.889$ Pa, $n = 0.4579$)	Transitional, Critical transition velocities	Critical velocity range detected (0.85–0.89 m/s); particle resuspension observed near transition.

the yield stress fluid exhibited drag reduction, and the axial turbulence intensities were higher near the wall compared to Newtonian fluids. The study also noted that the onset of transition in the yield stress fluid occurred in two stages, with initial fluctuations confined to the outer region of the flow before spreading throughout the section at higher Reynolds numbers.

As briefly discussed in the previous section, Güzel *et al.* (2009) conducted a detailed investigation into the transition behavior of non-Newtonian fluids. Using a combination of high-speed imaging and laser Doppler velocimetry (LDV), they measured parameters such as radial velocity, velocity fluctuations, and turbulence intensity profiles to map the transition process. Three different polymeric solutions were tested and characterized rheologically as Newtonian, PL, and HB fluids. Güzel observed that, in contrast to Newtonian fluids, non-

Newtonian fluids exhibit asymmetric velocity profiles during transition, with this asymmetry persisting until fully developed turbulence is reached (see Fig. 14). They attributed these asymmetries to the shear-thinning behavior of the fluids. During the transition, the leading edges of intermittent turbulent structures—puffs and slugs—were found to elongate and deviate from the pipe's central axis, while the trailing edges moved more slowly.

A similar observation has also been made in the recent experimental study by Charles *et al.* (2024), who investigated the transition flow of Carbopol solutions (modeled as HB fluid) in a cylindrical pipe. They employed a combination of pressure drop measurements and flow visualization techniques using a high-speed camera and reflective flake seeding. The authors identified a specific pre-transition regime, characterized by velocity profile asymmetry, which evolved with

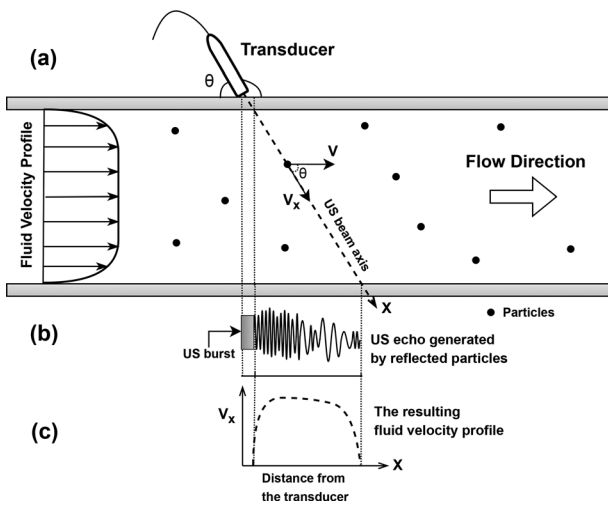


FIG. 15. Schematic representation of the ultrasonic velocity profiling (UVP) technique: (a) measurement system, (b) ultrasonic echo signal, and (c) measured velocity distribution.

increasing Reynolds number. Further, they observed a delay in the onset of turbulence, displaying a transition over a broader range. The author concluded that this delay is due to the presence of yield stress. However, the yield stress was not present in isolation, as the fluids also exhibited shear-thinning behavior. Consequently, the sole effect of yield stress on the transition process could not be definitively established. The details of these experimental studies are summarized in Table IV.

Despite their widespread use due to their reliability, extensive community support, robustness, and high temporal and spatial resolution, optical techniques are often restricted to optically transparent fluids and dilute slurries. In dense suspensions, particles, turbidity, and other factors that cause light scattering can severely restrict the applicability of these methods (Durst *et al.*, 1995; Ouriev and Windhab, 2002; and Poelma, 2020). Further, in highly concentrated slurries, the presence of seeding particles can exacerbate issues related to opacity and signal noise. Additionally, in these slurries, seeding particles may cluster, leading to inaccurate velocity measurements (Dash, 2022). For a more detailed discussion, readers can refer to Wright *et al.* (2017).

B. Acoustic methods

One of the significant advantages of acoustic methods, such as ultrasound-based techniques, is their ability to measure flow velocities in opaque fluids where optical methods like LDV and PIV are ineffective (Poelma, 2020). Researchers have attempted to address this limitation by using optically transparent slurries with similar rheological characteristics and employing techniques such as refractive index matching. Nevertheless, this approach is constrained to a limited range of material combinations, thereby restricting the physical parameter space available for investigation (Wiederseiner *et al.*, 2011). Ultrasound-based methods can be categorized into three groups: (1) time-of-flight methods, which measure the time it takes for an ultrasound pulse to travel between two points in a fluid, particularly effective for measuring mean flow velocities in flow meters; (2) Doppler-

based methods, also known as Ultrasonic Velocity Profiling (UVP) or Ultrasound Doppler Velocimetry (UDV), which measure the change in the ultrasound pulse as it is reflected by moving particles, providing the velocity component along the beam direction (Murakawa *et al.*, 2012) and (3) correlation-based techniques, also known as Ultrasound Imaging Velocimetry (UIV) or Echo-PIV, which involve applying cross correlation to ultrasound image data to estimate flow velocities (Poelma, 2017). The schematic of the ultrasound-based Doppler Velocity Profiling (UVP) technique in a pipe is presented in Fig. 15.

Although ultrasound-based methods have become increasingly popular in experimental research on multiphase flows [readers can refer to the review article by Tan *et al.* (2021)], only a limited number of studies have focused on single-phase viscoplastic fluids. For non-Newtonian HB fluids, Benslimane *et al.* (2016) investigated the laminar and turbulent flow behavior of bentonite suspensions at different concentrations (3.5%, 5%, and 8%), which were characterized as HB fluids. UDV was employed to determine the axial velocity distribution within a 20 mm diameter flow loop. Benslimane validated the experimental results against theoretical predictions for laminar flow and observed that the velocity profiles exhibited asymmetry during the transition phase. In the turbulent regime, the velocity profiles were found to align with the Dodge and Metzner (1959) correlation.

Krishnan Thota Radhakrishnan *et al.* (2021) used UIV to study the laminar-to-turbulent transition in non-settling kaolin slurries with concentrations up to 20% w/w, which were rheologically characterized as HB fluids, in a 0.1 m diameter pipeline. Using ultrasound imaging and time-averaged pressure drop measurements, they observed intermittent turbulent structures, such as puffs and slugs, during transitional flow in HB fluids (see Fig. 9).

This work was further extended by Dash (Dash and Poelma, 2022; Dash *et al.*, 2022), who focused on a single slurry with a concentration of 21% w/w, yield stress of 0.889 Pa, a consistency index of $0.1579 \text{ Pa}\cdot\text{s}^{0.4579}$, and a flow index of $n = 0.4579$. Experiments were conducted across a range of flow velocities (with a focus on transitional velocities), with critical transition velocities identified between 0.85 m/s and 0.89 m/s. The findings highlighted the presence of slow settling, where particles gradually settled under laminar flow conditions, and self-equilibration, where the flow adjusted to achieve full particle resuspension near the transition point. The study also focused on capturing turbulent velocity profiles in both the horizontal and vertical sections of the pipes at various flow velocities (Dash, 2022).

Ultrasound-based methods provide distinct advantages over optical techniques, particularly for opaque or turbid fluids. However, they do come with limitations, such as lower spatial and temporal resolution (Poelma, 2017; Dholakia *et al.*, 2020). In dense suspensions, the penetration depth of the ultrasound beam is significantly reduced due to attenuation (Fan and Wang, 2021). Further, most experimental studies (whether optical or acoustic) are only applicable to transitional or weakly turbulent flows. At industrially relevant high-turbulent flows, these experimental methods face additional constraints in terms of signal-to-noise ratio, difficulty in capturing fine-scale flow features, and reduced accuracy due to increased flow complexity and rapid fluctuations. To mitigate these challenges, researchers are exploring advanced approaches, including the use of higher-frequency transducers to enhance spatial resolution while managing the increased attenuation (Hyun *et al.*, 2019). Other strategies include developing more sensitive receivers with advanced signal processing to detect

weaker echoes from deeper within suspensions (Poelma, 2017) and employing multiple transducers at different angles (Gurung and Poelma, 2016). However, the effectiveness and applicability of these methods for purely viscous industrially relevant flows remain to be fully evaluated.

VI. SUMMARY AND DISCUSSION

This review highlights the recent advancements in modeling HB fluids in pipes, encompassing semi-empirical, computational, and experimental methods available in the literature. While the laminar flows of HB fluids can be modeled using first-principle physics, turbulence modeling remains challenging. Early developments relied on semi-empirical and theoretical approaches, often drawing analogies to Newtonian turbulence, such as the logarithmic velocity profile. While these models remain widely used in industrial applications, discrepancies between their predictions and experimental results persist, even when validated experimentally. These discrepancies are attributed to oversimplified assumptions during model formulation and the limited datasets used for model calibration.

More recent advancements in computational methods, particularly RANS modeling for non-Newtonian fluids, have introduced closures for three additional terms: Reynolds stresses, the model for average viscosity, and the fluctuating viscosity stress tensor. Incorporating these closures has notably improved turbulence predictions, underscoring the importance of non-Newtonian contributions to momentum and transport equations. However, this involves complex mathematical formulations with assumptions such as linear coupling between viscosity fluctuations and strain rates, neglect of higher-order nonlinear terms, and isotropic turbulence. Further, these models often rely on Newtonian-based constants, which require retuning for non-Newtonian scenarios. Additionally, the computational cost of these advanced closures restricts their application to flows in the early turbulence stages. Experimental evidence that shear-thinning and yield stress behaviors delay turbulence onset raises questions about the extent to which such flows achieve fully developed turbulence in practical scenarios, underscoring the need for further research.

An alternative approach simplifies the modeling process by disregarding the complexities of viscosity fluctuations and assuming their negligible impact on turbulence, except for adjustments near the walls. In these regions, simplified models, such as modified wall functions or damping functions, integrate fluid rheology to improve the accuracy of near-wall predictions. While this approach has shown considerable promise for highly turbulent flows, its effectiveness diminishes at lower turbulence levels. Moreover, much of the current research centers on PL fluids, as incorporating yield stress into the viscosity model introduces significant mathematical challenges, leaving gaps in modeling more complex non-Newtonian fluid behaviors.

Similar inconsistencies can also be observed under the transitional flows of non-Newtonian HB fluids. Experimental and simulation studies have shown that, unlike Newtonian fluids, the velocity profile of non-Newtonian fluids is asymmetric, and this asymmetry persists until there is a fully turbulent flow. Various theoretical and phenomenological criteria exist to define the transition or the critical point of onset of transition; however, large discrepancies have been observed when compared with experimental data. Stability-based methods, which rely on determining a stability parameter (the ratio of turbulent energy production to the rate of work done by viscous stress), have been proposed to be constant for all viscous fluids. However,

experimental studies have demonstrated that these parameters are sensitive to rheological characteristics and the fitted rheological model.

Similarly, Reynolds number-based methods have shown limited success, with prediction errors reaching up to 31% in some cases. This lack of consistency makes it difficult to establish a clear preference among the various predictive methods for non-Newtonian fluids. Further, for HB fluids, while various experimental studies have observed that transition is delayed, this is primarily attributed to their shear-thinning nature. Also, the role of the plug flow region, caused by yield stress, under a transition regime is often misunderstood and remains largely unexplored.

A significant reason for these inconsistencies is the limited availability of experimental data or high-fidelity DNS studies, which continues to hinder the development of more accurate models. DNS simulations are computationally expensive, limiting their application to transitional or weakly turbulent flows. On the other hand, most experimental studies reported in the literature focus on determining pressure loss or wall shear stress, while studies investigating detailed velocity profiles and turbulence statistics for HB fluids are rare. One of the prime reasons for this is the opaque nature of these non-Newtonian fluids. Optical experimental techniques, which are popular due to their high spatial and temporal resolution, could potentially be applied by using optically transparent slurries. However, this approach is limited to a narrow range of material combinations, restricting its broader applicability.

Acoustic-based methods offer a solution to opacity but face challenges like high sensitivity, low resolution, and attenuation, particularly in dense suspensions. Further, most experimental studies, whether optical or acoustic, are only applicable to transitional or weakly turbulent flows. At high turbulence, these methods face additional constraints, including a lower signal-to-noise ratio, difficulty in capturing fine-scale flow features, and reduced accuracy due to increased flow complexity and rapid fluctuations. These limitations impede progress in understanding transition and turbulence in non-Newtonian fluids, as the absence of detailed, high-resolution data, particularly near walls, hampers model validation, refinement, and the development of new theoretical frameworks.

Further, non-Newtonian fluid flow models, across all regimes, are sensitive to rheological characterization, as parameters derived from fitting curves can vary significantly depending on the rheometric method, shear rate range, and curve-fitting techniques. For instance, J. Singh (2016) has shown that the shear-rate range for rheological investigation should be at least two times the shear rate encountered in the wall shear stress measurements. However, this has largely been ignored in most rheological experiments. Similarly, Rooki *et al.* (2012), Chauhan *et al.* (2018), and various other studies have shown that the choice of fitting technique can lead to drastically different interpretations of fluid behavior.

For example, non-linear regression and other optimization techniques may result in zero or even negative yield stress values, effectively reducing an HB fluid model to a simpler PL fluid model. Also, effects such as viscoelasticity or thixotropy, which are frequently unaccounted for in standard models, can significantly influence flow behavior (Mitshita *et al.*, 2021). Further, non-Newtonian slurries, commonly assumed to be non-settling, often experience partial settling, which is generally ignored in experiments and simulations. Experimental studies also reveal that particles, including visualization

seeds, frequently agglomerate into flocs that settle over time, invalidating the pseudo-homogeneity assumption prevalent in numerical models.

Finally, amidst the discussion above, one factor of utmost importance but hitherto ignored is how one estimates the flow regime. The delayed transition to turbulence, influenced by shear-thinning and yield stress properties, challenges the reliability of existing Reynolds number models, which frequently fail to accurately predict this transition. For instance, recent experimental investigations by Charles *et al.* (2024) and Krishnan Thota Radhakrishnan *et al.* (2021) reported transition at $Re_w \approx 6260$ and $Re_w \approx 10\,500$, highlighting the inconsistencies in predictive models. Consequently, these modified Reynolds numbers lack universal applicability and require experimental validation. The absence of a similarity parameter, akin to the Reynolds number for Newtonian fluids, complicates the comparison and non-dimensionalization of the handful of experimental data sets available in the literature.

VII. FUTURE DIRECTIONS

Based on the review and the preceding discussion, it is evident that further fundamental research is crucial for advancing our understanding of non-Newtonian transition and turbulent flows. This deeper understanding is necessary to minimize the simplifications and assumptions currently made in the formulation of these models. There is a pressing need for more experimental data and DNS studies to accurately compute velocity profiles and turbulence statistics, which would allow for the verification of various modeling assumptions. For example, while linear coupling between fluctuating viscosity and strain rate simplifies modeling, it still requires experimental verification. This demands a more comprehensive set of experimental studies encompassing a wide range of pipe diameters, flow velocities, and fluid rheologies. This could be achieved by combining innovative acoustic approaches with advanced signal-processing techniques to capture detailed turbulence near the wall. This could also pave the way for data-driven approaches with the potential to capture complex behaviors where traditional models struggle.

Further, more comparative studies are needed to evaluate existing models comprehensively and provide guidelines for the design and development of operational envelopes. It is also possible that relying solely on wall shear stress may not be sufficient to assess the performance of these models. Detailed velocity and turbulence data may be necessary to reach more definitive conclusions. Finally, the role of the plug in HB fluids during the laminar-turbulent transition and in fully turbulent flows remains ambiguous. To understand this, detailed experimental investigations and DNS studies are essential, potentially focusing on the effects of shear-thinning and yield stress in isolation. This would also require more research in materials science, aiming to synthesize materials that exhibit these specific rheological properties independently while remaining affordable. These efforts will help to better understand the complexities of HB fluids in turbulent flow regimes and improve the accuracy of existing models.

ACKNOWLEDGMENTS

This article is the result of research conducted and funded by the Department of Water Management at Delft University of Technology, The Netherlands.

AUTHOR DECLARATIONS

Conflict of Interest

The authors have no conflicts to disclose.

Author Contributions

B. K. Yusufi: Conceptualization (lead); Methodology (lead); Writing – original draft (lead); Writing – review & editing (lead). **Z. Kapelan:** Project administration (equal); Supervision (equal); Writing – review & editing (equal). **D. Mehta:** Conceptualization (equal); Funding acquisition (lead); Investigation (lead); Resources (lead); Supervision (lead); Writing – review & editing (equal).

DATA AVAILABILITY

The data that support the findings of this study are available from the corresponding author upon reasonable request.

REFERENCES

- Alfonsi, G., “On direct numerical simulation of turbulent flows,” *Appl. Mech. Rev.* **64**(2), 020802 (2011).
- Alves, M. A., Oliveira, P. J., and Pinho, F. T., “Numerical methods for viscoelastic fluid flows,” *Annu. Rev. Fluid Mech.* **53**(1), 509–541 (2021).
- Amani, E., Ahmadvour, A., and Aghajari, M. J., “Large-eddy simulation of turbulent non-Newtonian flows: A comparison with state-of-the-art RANS closures,” *Int. J. Heat Fluid Flow* **99**, 109076 (2023).
- Ansys Fluent Theory Guide, ANSYS, Inc., release 2024 r2 edition, 2024. https://ansyshelp.ansys.com/public/account/secured?returnurl=/Views/Secured/corp/v242/en/flu_th/flu_th.html.
- Assefa, K. M. and Kaushal, D. R., “A comparative study of friction factor correlations for high concentrate slurry flow in smooth pipes,” *J. Hydrol. Hydromech.* **63**(1), 13 (2015).
- Barnes, H. A., “Thixotropy—A review,” *J. Non-Newtonian Fluid Mech.* **70**, 1–33 (1997).
- Bartosik, A., “Application of rheological models in prediction of turbulent slurry flow,” *Flow. Turbul. Combust.* **84**, 277–293 (2010).
- Basso, F. O., Franco, A. T., and Pitz, D. B., “Large-eddy simulation of turbulent pipe flow of Herschel-Bulkley fluids—assessing subgrid-scale models,” *Comput. Fluids* **244**, 105522 (2022).
- Bayareh, M., “An overview of non-Newtonian nanofluid flow in macro- and micro-channels using two-phase schemes,” *Eng. Anal. Boundary Elem.* **148**, 165–175 (2023).
- Benslimane, A., Bekkour, K., François, P., and Bechir, H., “Laminar and turbulent pipe flow of bentonite suspensions,” *J. Petroleum Sci. Eng.* **139**, 85–93 (2016).
- Bharathan, B., McGuinness, M., Kuhar, S., Kermani, M., Hassani, F. P., and Sasmito, A. P., “Pressure loss and friction factor in non-Newtonian mine paste backfill: Modelling, loop test and mine field data,” *Powder Technol.* **344**, 443–453 (2019).
- Bird, R. B., Armstrong, R. C., and Hassager, O., *Dynamics of Polymeric Liquids*. Volume 1. Fluid mechanics (John Wiley and Sons Inc., New York, NY, 1987).
- Blasius, H., “Das ähnlichkeitsgesetz bei reibungsvorgängen in flüssigkeiten,” in *Mitteilungen Über Forschungsarbeiten Auf Dem Gebiete Des Ingenieurwesens*, edited by Verein Deutscher Ingenieure (Springer, Berlin, Heidelberg, 1913), pp. 1–41. https://link.springer.com/chapter/10.1007/978-3-662-02239-9_1.
- Bogue, D. C. and Metzner, A. B., “Velocity profiles in turbulent pipe flow. Newtonian and non-Newtonian fluids,” *Ind. Eng. Chem. Fund.* **2**(2), 143–149 (1963).
- Bouffanais, R., “Advances and challenges of applied large-eddy simulation,” *Comput. Fluids* **39**(5), 735–738 (2010).
- Boussinesq, J., *Essai Sur la Théorie Des Eaux Courantes* (Gauthier-Villars, Paris, 1877). <https://archive.org/details/bpt6k9875921>.
- Bowen, R. L., “Chem. eng. 68 (july, 1961) 143,” *Chem. Eng.* **68**(July), 143 (1961).

- Busch, A., Myrseth, V., Khatibi, M., Skjetne, P., Hovda, S., and Johansen, S., "Rheological characterization of polyanionic cellulose solutions with application to drilling fluids and cuttings transport modeling," *Appl. Rheol.* **28**, 09 (2019).
- Carreau, P. J., De Kee, D. C. R., and Chhabra, R. P., "Rheology of polymeric systems," in *Rheology of Polymeric Systems* (Hanser, 2021a).
- Carreau, P. J., De Kee, D. C. R., and Chhabra, R. P., "Material functions and generalized Newtonian fluids," in *Rheology of Polymeric Systems*, edited by Pierre J. Carreau, Daniel C. R. De Kee, and Raj P. Chhabra, 2nd ed. (Hanser, 2021b), Chap. 2, pp. 21–68. ISBN 978–1-56990-722-1.
- Charles, A., Peixinho, J., Ribeiro, T., Azimi, S., Rocher, V., Baudez, J.-C., and Bahrani, S. A., "Asymmetry and intermittency in the rheo-inertial transition to turbulence in pipe flow," *Phys. Fluids* **36**(5), 054120 (2024).
- Chaudhuri, A., Wereley, N. M., Kotha, S., Radhakrishnan, R., and Sudarshan, T. S., "Viscometric characterization of cobalt nanoparticle-based magnetorheological fluids using genetic algorithms," *J. Magn. Magn. Mater.* **293**(1), 206–214 (2005).
- Chauhan, G., Verma, A., Das, A. *et al.*, "Rheological studies and optimization of Herschel-Bulkley flow parameters of viscous karaya polymer suspensions using GA and PSO algorithms," *Rheol. Acta* **57**, 267–285 (2018).
- Chhabra, R. P., *Non-Newtonian Fluids: An Introduction* (Springer, New York, NY, 2010), pp. 3–34. ISBN 978–1-4419–6494-6.
- Chhabra, R. P. and Richardson, J. F., *Non-Newtonian Flow and Applied Rheology* (Elsevier, 2008a).
- Chhabra, R. P., and Richardson, J. F., "Rheometry for non-Newtonian fluids," in *Non-Newtonian Flow and Applied Rheology*, 2nd ed., edited by R. P. Chhabra and J. F. Richardson (Butterworth-Heinemann, Oxford, 2008), Chap. 2, pp. 56–109. ISBN 978–0-7506–8532-0.
- Chilton, R. A. and Stainsby, R., "Pressure loss equations for laminar and turbulent non-Newtonian pipe flow," *J. Hydraul. Eng.* **124**(5), 522 (1998).
- Clapp, R. M., "Turbulent heat transfer in pseudoplastic non-Newtonian fluids," in *International Developments in Heat Transfer, ASME Part III, Section A* (ASME, 1961), p. 652.
- Colebrook, C. F., "Turbulent flow in pipes, with particular reference to the transition region between the smooth and rough pipe laws," *J. Inst. Civil Eng.* **11**(4), 133 (1939).
- Cruz, D. O. A. and Pinho, F. T., "Turbulent pipe flow predictions with a low Reynolds number $k-\epsilon$ model for drag reducing fluids," *J. Non-Newtonian Fluid Mech.* **114**(2–3), 109 (2003).
- Cruz, D. O. A., Pinho, F. T., and Resende, P. R., "Modelling the new stress for improved drag reduction predictions of viscoelastic pipe flow," *J. Non-Newtonian Fluid Mech.* **121**(2–3), 127 (2004).
- Csizmadia, P. and Hós, C., "CFD-based estimation and experiments on the loss coefficient for Bingham and power-law fluids through diffusers and elbows," *Comput. Fluids* **99**, 116–123 (2014).
- Dash, A., Hogendoorn, W., Oldenzel, G. *et al.*, "Ultrasound imaging velocimetry in particle-laden flows: Counteracting attenuation with correlation averaging," *Exp. Fluids* **63**, 56 (2022).
- Dash, A., "Opaque inertial suspensions," Ph.D. thesis (Delft University of Technology, 2022).
- Dash, A. and Poelma, C., "Long-time-scale transients in an industrial-scale slurry pipeline near the laminar-turbulent transition," *Flow* **2**, E25 (2022).
- Davidson, P., *Turbulence: An Introduction for Scientists and Engineers* (Oxford University Press, 2015). ISBN 9780198722588.
- Deng, X., "A mixed zero-equation and one-equation turbulence model in fluid-film thrust bearings," *J. Tribol.* **146**(3), 034101 (2024).
- Dewan, A., *Tackling Turbulent Flows in Engineering* (Springer Science & Business Media, 2011).
- Dholakia, K., Drinkwater, B. W., and Ritsch-Marte, M., "Comparing acoustic and optical forces for biomedical research," *Nat. Rev. Phys.* **2**(9), 480–491 (2020).
- Dodge, D. W. and Metzner, A. B., "Turbulent flow of non-Newtonian systems," *AIChE. J.* **5**(2), 189 (1959).
- Draad, A. A., Kuiken, G. D. C., and Nieuwstadt, F. T. M., "Laminar-turbulent transition in pipe flow for Newtonian and non-Newtonian fluids," *J. Fluid Mech.* **377**, 267 (1998).
- Durbin, P. A., "Separated flow computations with the k -epsilon- v -squared model," *AIAA J.* **33**(4), 659–664 (1995).
- Durst, F., Jovanović, J., and Sender, J., "Lda measurements in the near-wall region of a turbulent pipe flow," *J. Fluid Mech.* **295**, 305–335 (1995).
- Eckert, M., "Pipe flow: A gateway to turbulence," *Arch. Hist. Exact Sci.* **75**(3), 249 (2021).
- El-Emam, N., Kamel, A. H., El-Shafei, M., and El-Batrawy, A., "New equation calculates friction factor for turbulent flow on non-Newtonian fluids," *Oil Gas J.* **101**(36), 74–83 (2003).
- Erge, O., Ozbayoglu, E. M., Miska, S. Z., Yu, M., Takach, N., Saasen, A., and May, R., "Laminar to turbulent transition of yield power law fluids in annuli," *J. Petroleum Sci. Eng.* **128**, 128–139 (2015).
- Escudier, M. P. and Presti, F., "Pipe flow of a thixotropic liquid," *J. Non-Newtonian Fluid Mech.* **62**(2–3), 291 (1996).
- Escudier, M. P., Presti, F., and Smith, S., "Drag reduction in the turbulent pipe flow of polymers," *J. Non-Newtonian Fluid Mech.* **81**(3), 197–213 (1999).
- Eshtiagi, N., Markis, F., and Slatter, P., "The laminar/turbulent transition in a sludge pipeline," *Water Sci. Technol.* **65**(4), 697 (2012).
- Fan, J. and Wang, F., "Review of ultrasonic measurement methods for two-phase flow," *Rev. Sci. Instrum.* **92**(9), 091502 (2021).
- Fröhlich, J. and Rodi, W., "Introduction to large eddy simulation of turbulent flows," in *Closure Strategies for Turbulent and Transitional Flows* (Cambridge University Press, 2002), Vol. 1, pp. 197–224.
- Gavrilov, A. A., Finnikov, K. A., and Podryabinkin, E. V., "Modeling of steady Herschel-Bulkley fluid flow over a sphere," *J. Eng. Thermophys.* **26**, 197–215 (2017).
- Gavrilov, A. A. and Rudyak, V. Y., "Direct numerical simulation of the turbulent flows of power-law fluids in a circular pipe," *Thermophys. Aeromech.* **23**(4), 473–486 (2016a).
- Gavrilov, A. A. and Rudyak, V. Y., "Reynolds-averaged modeling of turbulent flows of power-law fluids," *J. Non-Newtonian Fluid Mech.* **227**, 45 (2016b).
- Gnambo, P. S., Orlandi, P., Ould-Rouiss, M., and Nicolas, X., "Large-eddy simulation of turbulent pipe flow of power-law fluids," *Int. J. Heat Fluid Flow* **54**, 196–210 (2015).
- Govier, G. W., Aziz, K., and Schowalter, W. R., "The flow of complex mixtures in pipes," *J. Appl. Mech.* **40**(2), 404 (1973).
- Gücüyener, I. H. and Mehmetog, T. *et al.*, "Characterization of flow regime in concentric annuli and pipes for yield-pseudoplastic fluids," *J. Petroleum Sci. Eng.* **16**(1–3), 45–60 (1996).
- Gul, S., Johnson, M. D., Karimi Vajargah, A., Ma, Z., Hoxha, B. B., and van Oort, E., "A data driven approach to predict frictional pressure losses in polymer-based fluids," in *SPE/IADC Drilling Conference, Proceedings* (2019), Vol. 2019.
- Gurung, A. and Poelma, C., "Measurement of turbulence statistics in single-phase and two-phase flows using ultrasound imaging velocimetry," *Exp. Fluids* **57**, 1–12 (2016).
- Güzel, B., Burghel, T., Frigaard, I. A., and Martinez, D. M., "Observation of laminar-turbulent transition of a yield stress fluid in Hagen-Poiseuille flow," *J. Fluid Mech.* **627**, 97 (2009).
- Haldenwang, R., Sutherland, A. P. N., Fester, V. G., Holm, R., and Chhabra, R. P., "Sludge pipe flow pressure drop prediction using composite power-law friction factor-Reynolds number correlations based on different non-Newtonian Reynolds numbers," *Water SA* **38**(4), 615–622 (2012).
- Hanjalic, K., *Closure Models for Incompressible Turbulent Flows* (Von Karman Institutes Fluid Dynamics, 2004), pp. 1–75. ISBN 2–930389–55–9.
- Hanjalic, K., "Will rans survive les? A view of perspectives," *J. Fluids Eng., Trans.* **127**, 831 (2005).
- Hanks, R. W., "The laminar-turbulent transition for fluids with a yield stress," *AIChE. J.* **9**(3), 306 (1963).
- Hanks, R. W., "A theory of laminar flow stability," *AIChE. J.* **15**(1), 25 (1969).
- Hanks, R. W., "Low Reynolds number turbulent pipeline flow of pseudohomogeneous slurries," in *Proceedings of the 5th International Conference on the Hydraulic Transport of Solids in Pipes*, Hannover, Germany (BHRA Fluid Engineering, 1978), pp. 22–34.
- Hanks, R. W. and Dadia, B. H., "Theoretical analysis of the turbulent flow of non-Newtonian slurries in pipes," *AIChE. J.* **17**(3), 554 (1971).

- Hanks, R. W. and Ricks, B. L., "Laminar-turbulent transition in flow of pseudo-plastic fluids with yield stresses," *J. Hydronaut.* **8**(4), 163–166 (1974).
- Hedström, B. O. A., "Flow of plastic materials in pipes," *Ind. Eng. Chem.* **44**(3), 651 (1952).
- Herschel, W. H. and Bulkley, R., "Konsistenzmessungen von Gummi-Benzollösungen," *Kolloid-Z.* **39**(4), 291 (1926).
- Heywood, N. I. and Cheng, D. C. H., "Comparison of methods for predicting head loss in turbulent pipe flow of non-Newtonian fluids," *Meas. Control* **6**(1), 33–45 (1984).
- Hogendoorn, W., Chandra, B., and Poelma, C., "Suspension dynamics in transitional pipe flow," *Phys. Rev. Fluids* **6**, 064301 (Jun 2021).
- Hyun, D., Li, Y. L., Steinberg, I., Jakovljevic, M., Klap, T., and Dahl, J. J., "An open source GPU-based beamformer for real-time ultrasound imaging and applications," in *Proceedings of the 2019 IEEE International Ultrasonics Symposium (IUS)* (IEEE, 2019), pp. 20–23.
- Jackson, D. and Launder, B., "Osborne Reynolds and the publication of his papers on turbulent flow," *Annu. Rev. Fluid Mech.* **39**, 19–35 (2007).
- Krishnan Thota Radhakrishnan, A., Poelma, C., van Lier, J., and Clemens, F., "Laminar-turbulent transition of a non-Newtonian fluid flow," *J. Hydraulic Res.* **59**(2), 235 (2021).
- Krishnan Thota Radhakrishnan, A., Van Lier, J., and Clemens, F., "Rheology of un-sieved concentrated domestic slurry: A wide gap approach," *Water* **10**(10), 1287 (2018).
- Kujawa-Roeleveld, K. and Zeeman, G., "Anaerobic treatment in decentralised and source-separation-based sanitation concepts," *Rev. Environ. Sci. Biotechnol.* **5**(1), 115 (2006).
- Lam, C. K. G. and Bremhorst, K., "A modified form of the $k-\epsilon$ model for predicting wall turbulence," *J. Fluids Eng., Trans.* **103**(3), 456 (1981).
- Larson, R. G. and Wei, Y., "A review of thixotropy and its rheological modeling," *J. Rheol.* **63**(3), 477 (2019).
- Launder, B. E. and Spalding, D. B., "The numerical computation of turbulent flows," *Comput. Methods Appl. Mech. Eng.* **3**(2), 269 (1974).
- Lazarus, J. H. and Slatter, P. T., "A method for the rheological characterisation of tube viscometer data," *J. Pipelines* **7**(2), 165–176 (1988).
- Livescu, S., "Mathematical modeling of thixotropic drilling mud and crude oil flow in wells and pipelines—A review," *J. Petroleum Sci. Eng.* **98–99**, 174–184 (2012).
- Lovato, S., Keetels, G. H., Toxopeus, S. L., and Settels, J. W., "An eddy-viscosity model for turbulent flows of Herschel–Bulkley fluids," *J. Non-Newtonian Fluid Mech.* **301**, 104729 (2022a).
- Lovato, S., Kirichek, A., Toxopeus, S. L., Settels, J. W., and Keetels, G. H., "Validation of the resistance of a plate moving through mud: CFD modelling and towing tank experiments," *Ocean Eng.* **258**, 111632 (2022b).
- Madlener, K., Frey, B., and Ciezki, H. K., "Generalized Reynolds number for non-Newtonian fluids," *Prog. Propul. Phys.* **1**, 237–250 (2009).
- Malin, M. R., "The turbulent flow of Bingham plastic fluids in smooth circular tubes," *Int. Commun. Heat Mass Transfer* **24**(6), 793 (1997a).
- Malin, M. R., "Turbulent pipe flow of power-law fluids," *Int. Commun. Heat Mass Transfer* **24**(7), 977 (1997b).
- Malin, M. R., "Turbulent pipe flow of Herschel–Bulkley fluids," *Int. Commun. Heat Mass Transfer* **25**(3), 321 (1998).
- Mehta, D., Van Zuijlen, A. H., Koren, B., Holierhoek, J. G., and Bijl, H., "Large eddy simulation of wind farm aerodynamics: A review," *J. Wind Eng. Ind. Aerodyn.* **133**, 1–17 (2014).
- Mehta, D., Krishnan Thota Radhakrishnan, A., van Lier, J., and Clemens, F., "A wall boundary condition for the simulation of a turbulent non-Newtonian domestic slurry in pipes," *Water (Switzerland)* **10**(2), 124 (2018a).
- Mehta, D., Krishnan Thota Radhakrishnan, A., van Lier, J., and Clemens, F., "Sensitivity analysis of a wall boundary condition for the turbulent pipe flow of Herschel–Bulkley fluids," *Water (Switzerland)* **11**(1), 19 (2018b).
- Mehta, D., Krishnan Thota Radhakrishnan, A., van Lier, J. B., and Clemens, F. H., "Assessment of numerical methods for estimating the wall shear stress in turbulent Herschel–Bulkley slurries in circular pipes," *J. Hydraulic Res.* **59**(2), 196 (2021).
- Menter, F. R., "Two-equation eddy-viscosity turbulence models for engineering applications," *AIAA J.* **32**(8), 1598–1605 (1994).
- Menter, F. R., Kuntz, M., Langtry, R. *et al.*, "Ten years of industrial experience with the SST turbulence model," *Turbul. Heat Mass Transfer* **4**(1), 625–632 (2003).
- Metzner, A. B. and Reed, J. C., "Flow of non-Newtonian fluids—correlation of the laminar, transition, and turbulent-flow regions," *AIChE J.* **1**(4), 434 (1955).
- Mewis, J., "Thixotropy—A general review," *J. Non-Newtonian Fluid Mech.* **6**(1), 1 (1979).
- Mishra, P. and Tripathi, G., "Transition from laminar to turbulent flow of purely viscous non-Newtonian fluids in tubes," *Chem. Eng. Sci.* **26**(6), 915 (1971).
- Mitishita, R. S., MacKenzie, J. A., Elfring, G. J., and Frigaard, I. A., "Fully turbulent flows of viscoplastic fluids in a rectangular duct," *J. Non-Newtonian Fluid Mech.* **293**, 104570 (2021).
- Moody, L. F., "Friction factors for pipe flow," *Trans. Am. Soc. Mech. Eng.* **66**, 671–681 (1944).
- Mooney, M., "Explicit formulas for slip and fluidity," *J. Rheol.* **2**(2), 210 (1931).
- Morrison, F. A., *Lezione Introductiva_Understanding Rheology* (Oxford University Press, 2001).
- Murakawa, H., Mori, M., and Takeda, Y., "Ultrasonic Doppler method," in *Ultrasonic Doppler Velocity Profiler Fluid Flow* (Springer, 2012), pp. 43–69.
- Nagano, Y. and Hishida, M., "Improved form of the $k-\epsilon$ model for wall turbulent shear flows," *J. Fluids Eng.* **109**(2), 156–160 (1987).
- Nikuradse, J., "Gesetzmäßigkeiten der turbulenten Strömung in glatten Röhren (Nachtrag)," *Forsch. Ing-Wes.* **4**(1), 44–44 (1933).
- Nishi, M., Ünsal, B., Durst, F., and Biswas, G., "Laminar-to-turbulent transition of pipe flows through puffs and slugs," *J. Fluid Mech.* **614**, 425 (2008).
- Nizamidin, N., "Optimized heavy oil-in-water emulsions for flow in pipelines," Ph.D. thesis, The University of Texas at Austin, Department of Petroleum and Geosystems Engineering, 2016.
- Ohta, T. and Miyashita, M., "DNS and LES with an extended Smagorinsky model for wall turbulence in non-Newtonian viscous fluids," *J. Non-Newtonian Fluid Mech.* **206**, 29–39 (2014).
- Oldroyd, J. G., "A rational formulation of the equations of plastic flow for a Bingham solid," *Math. Proc. Cambridge Philos. Soc.* **43**(1), 100–105 (1947).
- Ouriel, B. and Windhab, E. J., "Rheological study of concentrated suspensions in pressure-driven shear flow using a novel in-line ultrasound Doppler method," *Exp. Fluids* **32**, 204–211 (2002).
- Park, J. T., Mannheimer, R. J., Grimley, T. A., and Morrow, T. B., "Pipe flow measurements of a transparent non-Newtonian slurry," *J. Fluids Eng., Trans. ASME* **111**(3), 331 (1989a).
- Park, J. T., Mannheimer, R. J., Grimley, T. A., and Morrow, T. B., "Experiments on densely-loaded non-Newtonian slurries in laminar and turbulent pipe flows," Technical Report, Southwest Research Institute, San Antonio, TX, 1989b.
- Peixinho, J., Nouar, C., Desaubry, C., and Théron, B., "Laminar transitional and turbulent flow of yield stress fluid in a pipe," *J. Non-Newtonian Fluid Mech.* **128**(2–3), 172 (2005).
- Peric, M., "A finite volume method for the prediction of three-dimensional fluid flow in complex ducts," PhD thesis (University of London UK, 1985).
- Pinho, F. T., "A GNF framework for turbulent flow models of drag reducing fluids and proposal for a $k-\epsilon$ type closure," *J. Non-Newtonian Fluid Mech.* **114**(2–3), 149 (2003).
- Pinho, F. T., Li, C. F., Younis, B. A., and Sureshkumar, R., "A low Reynolds number turbulence closure for viscoelastic fluids," *J. Non-Newtonian Fluid Mech.* **154**(2–3), 89–108 (2008).
- Poelma, C., "Ultrasound imaging velocimetry: A review," *Exp. Fluids* **58**(1), 28 (2017).
- Poelma, C., "Measurement in opaque flows: A review of measurement techniques for dispersed multiphase flows," *Acta Mech.* **231**(6), 2089–2111 (2020).
- Pope, S. B., "Ten questions concerning the large-eddy simulation of turbulent flows," *New J. Phys.* **6**(1), 35 (2004).
- Prandtl, L., "Ueber die ausgebildete turbulenz," in *Proceedings 2nd International Congress Applied Mechanics, Zurich, 1926, Vol. 1217*, p. 62.
- Presti, F., "Investigation of transitional and turbulent pipe flow of non-Newtonian fluids," Ph.D. thesis, University of Liverpool, 2000. <https://livrepository.liverpool.ac.uk/id/eprint/3175053>.
- Rabinowitsch, B., "Über die viskosität und elastizität von solen," *Z. Physikalische Chem.* **145A**(1), 1 (1929).

- Rao, M. A., *Application of Rheology to Fluid Food Handling and Processing* (Springer US, Boston, MA, 2014), pp. 415–456. ISBN 978–1–4614–9230–6.
- Reed, T. D. and Pilehvari, A. A., “New model for laminar, transitional, and turbulent flow of drilling muds,” in *Production Operations Symposium* (1993).
- Rennels, D. C. and Hudson, H. M., *Pipe Flow: A Practical Comprehensive Guide* (John Wiley & Sons, 2012).
- Resende, P. R., Pinho, F. T., Younis, B. A., Kim, K., and Sureshkumar, R., “Development of a low-Reynolds-number $k\text{-}\omega$ model for fene-p fluids,” *Flow, Turbul. Combust.* **90**, 69–94 (2013).
- Rojas, D. A. and Janssen, R. H. A., “Design of open channels for non-Newtonian fluids,” in *Paste 2013: Proceedings of the 16th International Seminar on Paste and Thickened Tailings*, edited by R. Jewell, A. B. Fourie, J. Caldwell, and J. Pimenta (Australian Centre for Geomechanics, 2013), pp. 591–603.
- Rooki, R., Ardejani, F. D., Moradzadeh, A. *et al.*, “Optimal determination of rheological parameters for Herschel-Bulkley drilling fluids using genetic algorithms (gas),” *Korea-Aust. Rheol. J.* **24**, 163–170 (2012).
- Rudman, M. and Blackburn, H. M., “Direct numerical simulation of turbulent non-Newtonian flow using a spectral element method,” *Appl. Math. Modell.* **30**(11), 1229 (2006).
- Rudman, M., Blackburn, H. M., Graham, L. J. W., and Pullum, L., “Turbulent pipe flow of shear-thinning fluids,” *J. Non-Newtonian Fluid Mech.* **118**(1), 33 (2004).
- Ryan, N. W. and Johnson, M. M., “Transition from laminar to turbulent flow in pipes,” *AIChE. J.* **5**(4), 433 (1959).
- Sawko, R., “Mathematical and computational methods of non-Newtonian, multiphase flows,” Ph.D. thesis (Cranfield University, 2012). <http://dspace.lib.cranfield.ac.uk/handle/1826/7264>.
- Silva, R. C., “Experimental characterization techniques for solid-liquid slurry flows in pipelines: A review,” *Processes* **10**(3), 597 (2022).
- Singh, J., “The importance of rheology characterization in predicting turbulent pipe flow of generalized Newtonian fluids,” *J. Non-Newtonian Fluid Mech.* **232**, 11–21 (2016).
- Singh, J., Rudman, M., and Blackburn, H. M., “The influence of shear-dependent rheology on turbulent pipe flow,” *J. Fluid Mech.* **822**, 848 (2017a).
- Singh, J., Rudman, M., and Blackburn, H. M., “The effect of yield stress on pipe flow turbulence for generalised Newtonian fluids,” *J. Non-Newtonian Fluid Mech.* **249**, 53 (2017b).
- Singh, J., Rudman, M., and Blackburn, H. M., “Reynolds number effects in pipe flow turbulence of generalized Newtonian fluids,” *Phys. Rev. Fluids* **3**(9), 094607 (2018).
- Skelland, A. H. P., *Non-Newtonian Flow and Heat Transfer* (John Wiley & Sons, 1967).
- Slatter, P. T., “Modelling the turbulent flow of non-Newtonian slurries,” *R&D J.* **12**(2), 68–80 (1996).
- Slatter, P. T., “The laminar/turbulent transition of non-Newtonian slurries in pipes,” in *14th World Dredging Congress*, 1995, pp. 31–48.
- Sorgun, M., Muftuoglu, T. D., and Gucuyener, I. H., “Friction factor estimation for turbulent flow of Herschel-Bulkley and power law fluids in pipes,” *J. Petroleum Sci. Eng.* **211**, 110044(2022).
- Szilas, A. P., Bobok, E., and Navratil, L., “Determination of turbulent pressure loss of non-Newtonian oil flow in rough pipes,” *Rheol. Acta* **20**(5), 487 (1981).
- Taghvaei, M. and Amani, E., “Wall-modeled large-eddy simulation of turbulent non-Newtonian power-law fluid flows,” *J. Non-Newtonian Fluid Mech.* **322**, 105136 (2023).
- Tan, C., Murai, Y., Liu, W., Tasaka, Y., Dong, F., and Takeda, Y., “Ultrasonic Doppler technique for application to multiphase flows: A review,” *Int. J. Multiphase Flow* **144**, 103811 (2021).
- Thomas, A. D. and Wilson, K. C., “New analysis of non-Newtonian turbulent flowdashyield-power-law fluids,” *Can. J. Chem. Eng.* **65**(2), 335 (1987).
- Todt, D., Bisschops, I., Chatzopoulos, P., and Van Eekert, M. H. A., “Practical performance and user experience of novel DUAL-Flush vacuum toilets,” *Water (Switzerland)* **13**(16), 2228 (2021).
- Tomita, Y., “A study on non-Newtonian flow in pipe lines,” *Bull. JSME* **2**(5), 10 (1959).
- Torrance, B. M., “Friction factors for turbulent non-Newtonian fluid flow in circular pipes,” *South Afr. Mech. Eng.* **13**, 89–91 (1963).
- Tsukahara, T., Ishigami, T., Yu, B., and Kawaguchi, Y., “Dns study on viscoelastic effect in drag-reduced turbulent channel flow,” *J. Turbul.* **12**, N13 (2011).
- Van den Heever, E. M., Sutherland, A. P. N., and Haldenwang, R., “Influence of the rheological model used in pipe-flow prediction techniques for homogeneous non-Newtonian fluids,” *J. Hydraul. Eng.* **140**(12), 04014059 (2014).
- Visintainer, R., Matoušek, V., Pullum, L., and Sellgren, A., *Practical Experience with Slurry Systems* (Springer International Publishing, Cham, 2023), pp. 317–359. ISBN 978–3–031–25440–6.
- Messa, G. V., Yang, Q., Adedeji, O. E., Chára, Z., Antonio Ribeiro Duarte, C., Matoušek, V., Rasteiro, M. G., Sanders, R. S., Silva, R. C., and De Souza, F. J., “Computational fluid dynamics modelling of liquid–solid slurry flows in pipelines: State-of-the-art and future perspectives,” *Processes* **9**(9), 1566 (2021).
- von Kármán, T., *Mechanical Similitude and Turbulence* (National Advisory Committee for Aeronautics, 1931), No. 611.
- Wang, L., Cheng, L., Yin, S., Yan, Z., and Zhang, X., “Multiphase slurry flow regimes and its pipeline transportation of underground backfill in metal mine: Mini review,” *Constr. Build. Mater.* **402**, 133014 (2023).
- Wiederseiner, S., Andreini, N., Epely-Chauvin, G., and Ancey, C., “Refractive-index and density matching in concentrated particle suspensions: A review,” *Exp. Fluids* **50**, 1183–1206 (2011).
- Wilcox, D. C., “Reassessment of the scale-determining equation for advanced turbulence models,” *AIAA J.* **26**(11), 1299 (1988).
- Wilcox, D. C., *Turbulence Modeling for CFD*, 3rd ed. (DCW Industries, Canada, CA, USA, 2006), Vol. 1.
- Wilson, K. C. and Thomas, A. D., “A new analysis of the turbulent flow of non-Newtonian fluids,” *Can. J. Chem. Eng.* **63**(4), 539 (1985).
- Wright, S. F., Zadrzil, I., and Markides, C. N., “A review of solid–fluid selection options for optical-based measurements in single-phase liquid, two-phase liquid–liquid and multiphase solid–liquid flows,” *Exp. Fluids* **58**, 1–39 (2017).
- Wyganski, I., Sokolov, M., and Friedman, D., “On transition in a pipe. Part 2. The equilibrium puff,” *J. Fluid Mech.* **69**(2), 283 (1975).
- Wyganski, I. J. and Champagne, F. H., “On transition in a pipe. Part 1. The origin of puffs and slugs and the flow in a turbulent slug,” *J. Fluid Mech.* **59**(2), 281 (1973).
- Xu, J., Gillies, R., Small, M., and Shook, C. A., “Laminar and turbulent flow of kaolin slurries,” in *12th International Conference on Slurry Handling and Pipeline Transport, Hydrotransport 12* (BHR Group, 1993), pp. 595–613.
- Yousuf, N., Kurukulasuriya, N., Chryss, A., Rudman, M., Rees, C., Usher, S., Farno, E., Lester, D., and Eshtiaghi, N., “An accurate and robust method for intensification of wastewater sludge pipe flow,” *Sci. Total Environ.* **949**, 175143 (2024).
- Yusufi, B. K., Kapelan, Z., and Mehta, D., “Rheology-based wall function approach for wall-bounded turbulent flows of Herschel–Bulkley fluids,” *Phys. Fluids* **36**(2), 023112 (2024).
- Zheng, E. Z., Rudman, M., Singh, J., and Kuang, S. B., “Direct numerical simulation of turbulent non-Newtonian flow using openfoam,” *Appl. Math. Modell.* **72**, 50–67 (2019).